NASA-TM-72867 19790023049

NASA Technical Memorandum 72867

ANALYSIS OF A LATERAL PILOT-INDUCED OSCILLATION EXPERIENCED

ON THE FIRST FLIGHT OF THE YF-16 AIRCRAFT

John W. Smith

September 1979
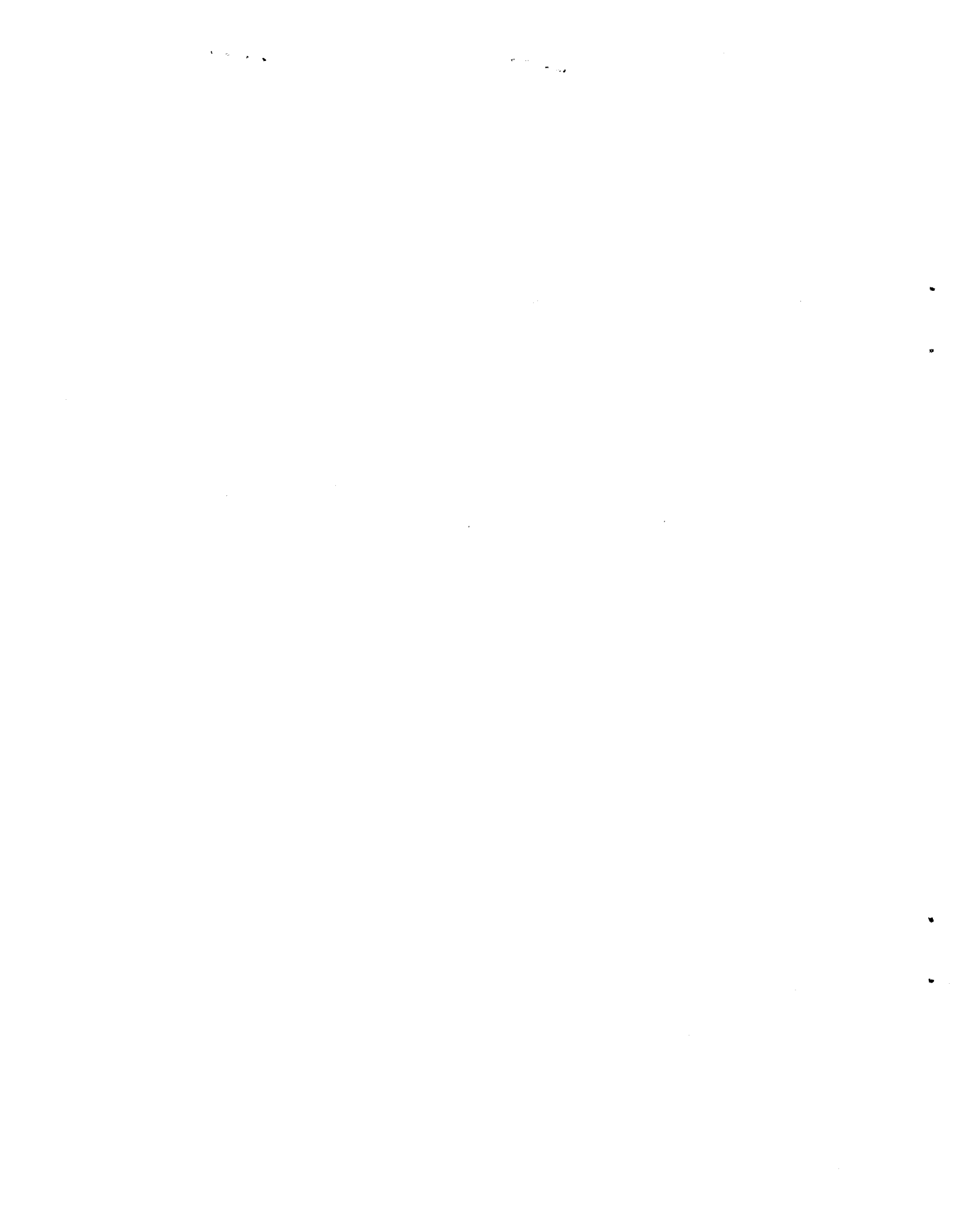
NASA

NASA Technical Memorandum 72867

ANALYSIS OF A LATERAL PILOT-INDUCED OSCILLATION EXPERIENCED

ON THE FIRST FLIGHT OF THE YF-16 AIRCRAFT

John W. Smith

Dryden Flight Research Center
Edwards, California

NASA
National Aeronautics and
Space Administration

1979
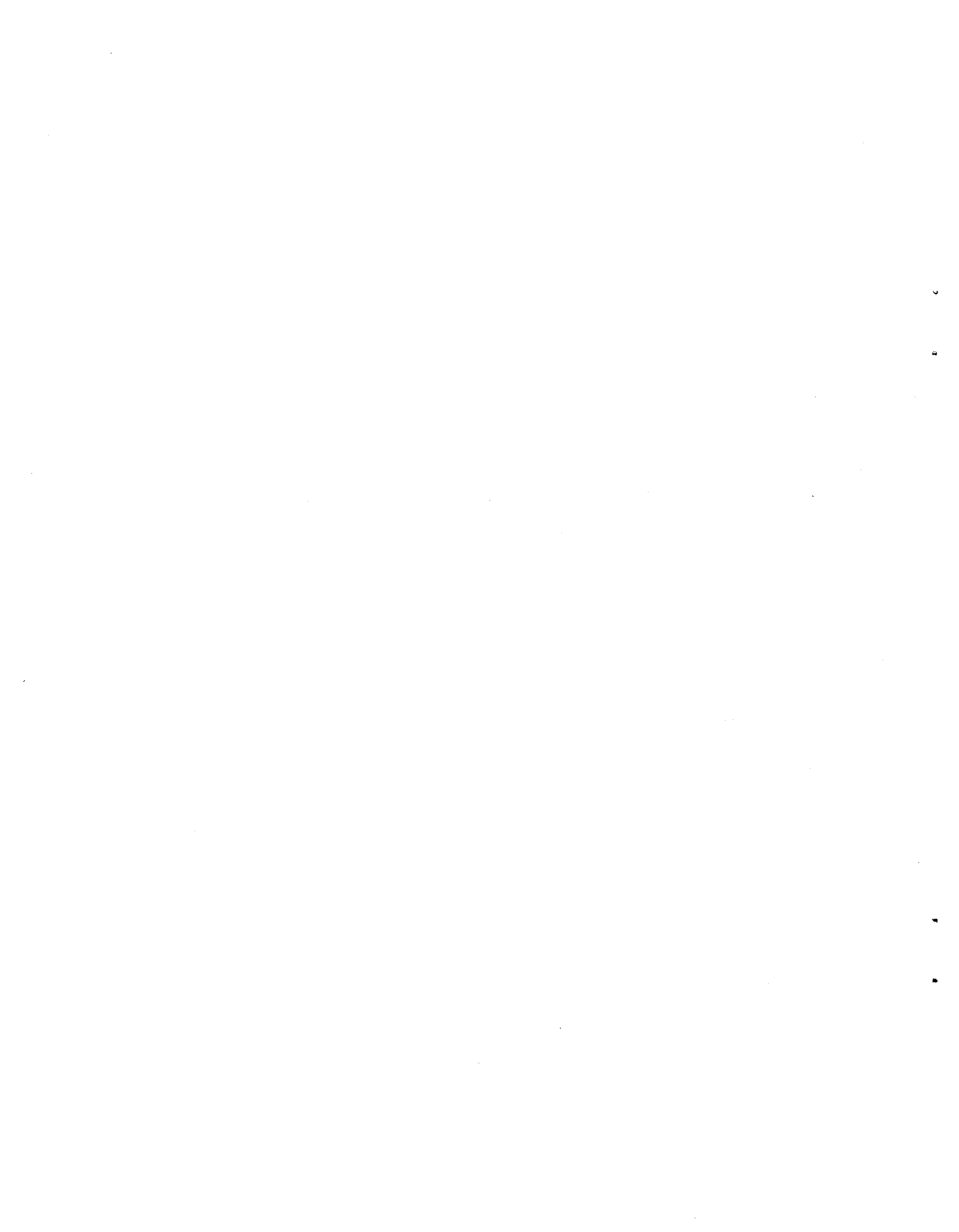
ANALYSIS OF A LATERAL PILOT-INDUCED

OSCILLATION EXPERIENCED ON THE

FIRST FLIGHT OF THE YF-16 AIRCRAFT

John W. Smith
Dryden Flight Research Center

INTRODUCTION

During a first flight, or early in the flight test program of new aircraft, numerous incidents of pilot induced oscillations (PIO's) have occurred (ref. 1). In a majority of the cases, the occurrence has been about the longitudinal axis, such as in the experiences reported and analyzed in reference 2. However, the pilot can also develop and sustain a PIO in maintaining roll attitude control.

During a high speed taxi run, scheduled as part of the buildup prior to the first flight, the YF-16 aircraft inadvertently became completely airborne; this necessitated a complete go-around. The test plan called for a taxi run to peak speed, and a minimum lift-off, to be followed by a slight lateral control input. However, a fairly high frequency PIO (.7 cycle per second) occurred on lift-off and was sustained for 12 complete cycles. As a result, the aircraft became misalined with the remaining runway. The pilot, therefore, was compelled to add power and complete the takeoff (appendix A). The magnitude and rate of the pilot roll control inputs were sufficient to position and rate saturate the roll control system.

The PIO occurrence was reported by the Air Force in reference 3. This experience, plus the studies conducted by the contractor, led to a system design change which in general reduced the overall lateral control system gain for the takeoff and landing phases. The interim system that was implemented, following this first flight, is identified in this report as the modified flight control system (MFCS).

Despite the long history of PIO's, a generally valid prediction technique does not exist. One of the means available to designers for their prevention is to compare the characteristics of new aircraft with the characteristics of aircraft that have proved to be resistant or prone to these oscillations.

Because the YF-16 has a highly advanced fly-by-wire control system, a study of its PIO situation would contribute to the body of knowledge on aircraft PIO characteristics. Consequently a study was initiated to investigate the integrated control characteristics of the aircraft, control system, and pilot. The problem was approached and analyzed initially in a linear fashion with and without ground effects included. Nonlinear analytical studies were

utilized to predict the frequency responses under saturated conditions and used to compare the initial control system to the MFCS control system with and without ground effects.

This report discusses the theoretical analyses made at the Dryden Flight Research Center regarding this PIO occurrence on the YF-16 prototype airplane.

SYMBOLS AND ABBREVIATIONS

Physical quantities in this report are given in the International System of Units (SI) and parenthetically in U.S. Customary Units. The measurements were taken in U.S. Customary Units. Factors relating the two systems are presented in reference 4.

A	amplitude
A/C	aircraft
A/C(s)	aircraft transfer function
A_H	actuator
a_y	lateral acceleration, g
b	reference span, m (ft)
C	generalized control output
C_ℓ	rolling-moment coefficient, $\dfrac{\text{Rolling moment}}{qsb}$
C_{ℓ_p}	roll-damping derivative, $\dfrac{\partial C_\ell}{\partial \frac{pb}{V}}$, rad^{-1}
C_{ℓ_r}	rolling moment due to yaw rate, $\dfrac{\partial C_\ell}{\partial \frac{pb}{2V}}$, rad^{-1}
C_{ℓ_β}	effective dihedral derivative, $\dfrac{\partial C_\ell}{\partial \beta}$, deg^{-1}

$C_{l_{\delta_a}}$ horizontal tail-roll effectiveness derivative, $\dfrac{\partial C_l}{\partial \delta_a}$, deg^{-1}

$C_{l_{\delta_F}}$ flaperon-roll effectiveness derivative, $\dfrac{\partial C_l}{\partial \delta_F}$, deg^{-1}

$C_{l_{\delta_r}}$ rolling moment due to rudder deflection, $\dfrac{\partial C_l}{\partial \delta_r}$, deg^{-1}

$C_{l_{\phi}}$ rolling moment due to ground effect, $\dfrac{\partial C_l}{\partial \phi}$, rad^{-1}

C_n yawing-moment coefficient, $\dfrac{\text{Yawing moment}}{qsb}$

C_{n_p} yawing-moment due to roll rate, $\dfrac{\partial C_n}{\partial \frac{pb}{2V}}$, rad^{-1}

C_{n_r} yaw-damping derivative, $\dfrac{\partial C_n}{\partial \frac{rb}{2V}}$, rad^{-1}

$C_{n_{\beta}}$ directional-stability derivative, $\dfrac{\partial C_n}{\partial \beta}$, deg^{-1}

$C_{n_{\delta_a}}$ yawing moment due to aileron deflection, $\dfrac{\partial C_n}{\partial \delta_a}$, deg^{-1}

$C_{n_{\delta_F}}$ yawing moment due to flaperon deflection, $\dfrac{\partial C_n}{\partial \delta_F}$, deg^{-1}

$C_{n_{\delta_r}}$ rudder-effectiveness derivative, $\dfrac{\partial C_n}{\partial \delta_r}$, deg^{-1}

C_{n_ϕ} yawing moment due to ground effect, $\dfrac{\partial C_n}{\partial \phi}$, rad^{-1}

C_Y side-force coefficient, $\dfrac{Side\ force}{qs}$

C_{Y_p} side-force derivative, $\dfrac{\partial C_y}{\partial p}$, deg^{-1}

C_{Y_r} side-force derivative, $\dfrac{\partial C_Y}{\partial r}$, deg^{-1}

C_{Y_β} side-force derivative, $\dfrac{\partial Y}{\partial \beta}$, deg^{-1}

$C_{Y_{\delta_a}}$ side force due to aileron deflection, $\dfrac{\partial C_Y}{\partial \delta_a}$, deg^{-1}

$C_{Y_{\delta_F}}$ side force due to flaperon deflection, $\dfrac{\partial C_Y}{\partial \delta_F}$, deg^{-1}

$C_{Y_{\delta_r}}$ side force due to rudder deflection, $\dfrac{\partial C_Y}{\partial \delta_r}$, deg^{-1}

C_{Y_ϕ} side-force derivative due to ground effect, $\dfrac{\partial C_Y}{\partial \phi}$, deg^{-1}

$\bar{c}$ mean aerodynamic chord, m (ft)

D	denominator
DN	down
e	error signal, rad or deg
F	flaperon
F_a	lateral stick force, kg (lb)
F_a/ϕ_e	pilot gain, kg/rad (lb/rad)
f( )	function of parameter inside the parentheses
G_H	horizontal tail forward loop transfer function
G_F	flaperon forward loop transfer function
G_r	rudder forward loop transfer function
g	acceleration due to gravity, 9.8 m/sec^2 (32.2 ft/sec^2)
H_p	roll rate feedback transfer function
H_r	yaw rate feedback transfer function
H_y	lateral acceleration feedback transfer function
H(s)	feedback transfer function
HT	horizontal tail
h	altitude, m (ft)
I_x, I_z	vehicle moments of inertia about the x- and z-body axes, respectively, kg-m^2 (slug-ft^2)
I_{xz}	product of inertias, kg-m^2 (slug-ft^2)
jω	imaginary part of Laplace transform variable, rad/sec

K	gain constant
KN	gain constant with a limit
K_p	roll rate gain
K_ϕ	roll attitude gain
LEF	leading edge flaps
M	Mach number
MAC	mean aerodynamic chord
MFCS	modified flight control system
N	numerator
PIO	pilot-induced oscillation
p	rolling angular rate, rad/sec
q	dynamic pressure, N/m^2 (lb/ft^2)
R	generalized input
r	yawing angular rate, rad/sec
S	reference planform area, m^2 (ft^2)
SAS	stability augmentation system
s	Laplace transform variable, $(\sigma + j\omega)$, rad/sec
T(s)	transfer function
TEF	trailing edge flap
t	time, sec
V	true airspeed, m/sec (ft/sec)
W	weight, kg (lb)
X	input or output quantity
Y(s)	generalized transfer function
α	angle of attack, deg

β	angle of sideslip, deg
Δ	transfer function denominator
δ_a	differential horizontal tail deflection, $\frac{1}{2}(\delta_{HT/R} - \delta_{HT/L})$ deg or rad
δ_F	differential flaperon deflection, $\frac{1}{2}(\delta_{F/R} - \delta_{F/L})$, deg or rad
δ_r	rudder deflection, deg or rad
ζ	damping ratio of second-order response
σ	real part of Laplace transform variable, rad/sec
ϕ	angle of bank, rad
ϕ/F_a	system gain, rad/N (rad/lb)
ϕ	phase angle, deg
ω	frequency, rad/sec

Subscripts:

cr	critical
c	commanded
e	error signal
H	hydraulic
HT	horizontal tail
L	left
n	natural
R	right
R	generalized input
X, Y, Z	vehicle body axis

1, 2, 3,....   sequential calculation in the order indicated.

A dot over a quantity denotes the first derivative with respect to time.

VEHICLE DESCRIPTION

Aircraft

The YF-16 aircraft, under Air Force contract, was designed and manufactured by the General Dynamics Convair Aerospace Division of Fort Worth, Texas. The aircraft is a prototype lightweight fighter designed to have high g maneuverability plus supersonic speed capability. Shown in figure 1 is a three-view drawing illustrating the relative size and location of the primary control surfaces. The pertinent physical characteristics of the aircraft are presented in table 1.

Primary and Secondary Flight Control Systems

Aerodynamic surfaces. - Flightpath control in pitch and roll is achieved by a differential all-movable horizontal tail. Additional roll control is provided by wing-mounted flaperons. Directional control is accomplished by a conventional rudder mounted on the trailing edge of a single vertical stabilizer.

Fly by wire. - A full fly-by-wire system is utilized in all three axes. The system is quadruple redundant as to the sensors and the electrical output of the pilot controller, computers, and electronic circuitry. The mechanical inputs to control surface power actuators are provided by the electromechanical command servos and are single-fail-operate components.

Secondary systems. - Leading-edge flaps are provided for takeoff, landing, and high angle of attack maneuvers. The leading-edge flaps are also scheduled as a function of angle of attack. Speed brakes located inboard of the horizontal tail provide deceleration capability.

Pilot controls and augmentation. - Through a minimum displacement force sidearm controller, the pilot provides pitch and roll inputs to a rate command augmentation system, rather than controlling surface positions directly. Longitudinal force inputs command a blend of pitch rate and normal acceleration. The pitch feedback loops attempt to provide response characteristics that are almost invariant with flight condition. Lateral force commands roll rate proportional to the error signal (fig. 2). Favorable roll-yaw coordination is accomplished through the angle of attack range by an aileron-rudder interconnect.

A typical stability augmentation system (SAS) is implemented in the yaw axis and summed with rudder pedal position to provide both dynamic and static stability. Aircraft dynamic stability is augmented by a washed-out yaw rate feedback. Static directional stability is augmented by a lateral acceleration feedback. The surface authorities and rate limits are presented in table 2.

A more complete description of the total flight control system and its design is given in reference 5.

Instrumentation

The YF-16 instrumentation (ref. 3) was designed, installed, and maintained by General Dynamics. The data presented in this report were recorded on board by a pulse code modulation system at 40 samples per second. The data system is considered to be accurate to within 3 percent of full-scale range of the parameter being recorded.

ANALYSIS AND DISCUSSION

YF-16 PIO Experience

Throughout the design and manufacturing phases of the prototype aircraft, the flight control systems underwent design, development, and testing on both fixed base and in-flight simulators. During these tests, the augmentation systems were integrated with the basic aircraft response characteristics to produce excellent flying qualities throughout the airplane's flight envelope. In addition, the feel characteristics (roll rate per stick force) selected and implemented were those felt to be the most desirable. However, as only natural, simulator studies motivate less attentive controlling or piloting than actually flying the aircraft. Therefore, it is highly likely that pilot gain can be much higher during flight testing than during any type of simulator flying, especially on the first flight.

Consequently, on the first flight of the YF-16 aircraft, which was scheduled as a high speed taxi run, the pilot experienced a severe PIO immediately upon lift-off (appendix A). The magnitude and rate of the roll control input by the pilot was sufficient to position and rate saturate the roll control system. The normal system lag and a constant lag due primarily to rate saturation introduced enough total system lag at the input frequency and amplitude to cause the pilot's lateral stick input/output relationship to be 180 degrees or more out of phase with the estimated peak bank angles. Table 3 lists the flight conditions of the aircraft during the PIO.

Figure 3 presents a time history of the PIO experienced during takeoff on the first flight (from ref. 3). The parameters shown are lateral stick force, lateral control surface positions, and roll rate. As indicated by the saturation of the lateral stick force transducer trace, F_a, maximum roll rate was commanded. The flaperons were the only control surfaces exhibiting continuous rate limiting during the PIO, as indicated by the triangular wave shape. The maximum rate for the sum of the two flaperon surfaces was approximately 112 degrees per second (approximately twice the individual surface rate limits (table 2)), at a frequency of .67 cycle per second, and was sustained for approximately 12 complete cycles. For most of the cycles, the aircraft roll rates reached average peak values of about ±50 degrees per second, and bank angles were estimated to be ±15 degrees. Presented in table 4 is a summary of the pertinent characteristics of the PIO which were determined from an analysis of the time history. Also listed in the table are conditions common to other PIO's and unique features of the YF-16 system.

9

Roll Control Modeling

The discussion that follows defines the modeling aspects and analytical description of the roll control mode for the YF-16 aircraft.

System description and control elements. - Presented in figure 4 is a block diagram representation of the lateral control loops, including the pilot, that is suitable for both the linear and nonlinear PIO analysis. The pilot attempts to minimize the aircraft bank angle error to a wings-level position. The amount of force he applies per unit error signal is referred to as pilot gain. The original system roll command force gradient, dual lag filter, and actuator response descriptions are presented in figures 5 to 7. The roll stick force command gradient is described by a cubic equation shown by the dashed line in figure 5. The dual lag command prefilter consists of four nonlinearities (fig. 6), two in each feedback path. In each feedback path and in between the nonlinearities is a washout network which allows the affected loop to null when commands have a constant value. The purpose of this filter is to command a faster response initially and then a somewhat slower response as the error signal (e) approaches zero. However, the average phase lag per cycle can be closely matched by just the forward loop transfer function ($\frac{10}{s + 10}$) if sine wave amplitudes limited to that of the saturated input are used in the mathematical model.

At a flap setting of 20 degrees, the flaperons are at the full down deflection limit. A flap crossfeed logic utilizing the limiters and thresholds (fig. 2) maintains the gain of the roll control channel by doubling the deflection of the upward moving flaperon to compensate for the lack of a downward-moving flaperon on the opposite side. Also, whenever the surfaces were moving in opposite directions, the total rate limiting would be twice the rate limiting exhibited by a single surface (approximately 112 deg/sec). A diagram typical of the mechanical servos and actuators is presented in figure 7. The system rates, authorities, and servo characteristics for each system affecting roll response are presented in table 2. Rate limiting can be approximated with reference to figure 7 by using the following system. The restraint of any gain change is considered to be just in the forward loop of power actuator servos, and not in the feedback loop.
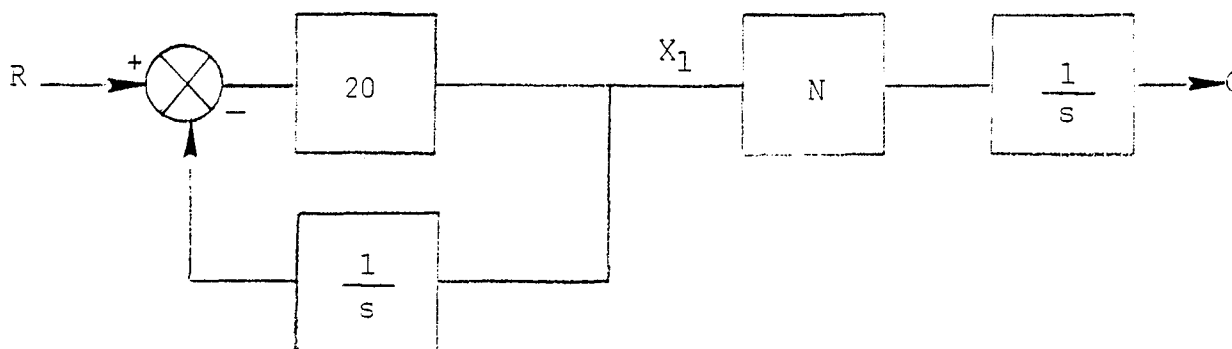
$$X_1 = \left(\frac{20}{s + 20} \right) s \times R$$

or C, the output, would be

$$C = X_1 \, N \times \frac{1}{s}$$

where the rate restriction N is

$$0 \leq X_1 \leq \frac{60}{57.3}$$

Since the change in feedback gain due to the nonlinearity is neglected, this makes the closed-loop input/output relationship for saturated inputs slightly smaller than the actual system at the lower frequencies of interest ($\omega < 8$ rad/sec).

The differential horizontal tail was unaffected, since surface limiting due to roll command in that path was not prevalent during the PIO.

Modified flight control system. - Following the PIO experienced on the first flight, the YF-16 aircraft's roll control system was modified to include a takeoff and land mode. In general, these modifications reduce the system gain in the forward loop, reduce the roll command force gradient, and lower the maximum roll rate that can be commanded. In this report, this system is designated as the modified flight control system (MFCS).

Presented in figure 8 is the roll command gradient implemented on the MFCS. The dashed line indicates the cubic equation in the subsequent studies that was used to define the roll rate commanded per lateral stick force. Maximum commanded roll rate was limited to 167 degrees per second. The forward loop gain, KN, of the roll control system was reduced from 0.20 for the original system to 0.12 radian/radian per second for the MFCS (fig. 4).

Aerodynamic characteristics. - The aerodynamic stability and control derivatives were obtained from rigid model tests conducted in wind tunnels at various facilities. The data were compiled and reported in reference 6. Table 5 lists the pertinent coefficients as transferred to the body axis. The transfer functions ratioing roll rate to surface deflection were obtained by using typical computer programs and the appropriate geometry and flight conditions (tables 1 and 3).

Ground effects. - Airplanes flying near the ground plane during takeoff and landing experience changes in aerodynamics forces and moments that are termed ground effects. Many studies have been made regarding these effects, but they have addressed primarily the changes in forces and moments about the longitudinal axis. The studies have shown that near the ground plane the overall effect is an increase in lift, a decrease in pitching moment, and a reduction in drag force.

Lateral and directional changes in moments are for the most part considered small, because the bank angle is usually near zero. However, if the bank angle becomes relatively large (ϕ = 15 deg or greater), the change in pressure distribution may be large enough to affect the lateral dynamics. The extent of these effects, particularly regarding the flying qualities, would, of course, depend on the type and amount of stability augmentation.

To complement these studies, and because this PIO was in the ground effect regime, an estimate was inserted in the equations of motion to account for these changes in the lateral forces and moments.

Datcom (ref. 7), which is a compilation of design information previously published in theoretical reports, presents a section on methods of estimating the changes in longitudinal forces and moments as a function of height above the ground level. In this report, the estimates utilize the same information except that bank angle is related to the height difference between the right and left wing quarter-chord-of-the-MAC. Thus, the difference in lift force would cause a resultant rolling and yawing moment component. For a bank angle of 15 degrees and an average height of 2.74 meters (9 feet), it was estimated that:

$$C_{\ell_\phi} = -.026 \text{ per radian}$$

$$C_{n_\phi} = .00635 \text{ per radian}$$

$$C_{Y_\phi} = 1.376 \text{ per radian}$$

The transfer functions including these additional terms are presented along with the basic aerodynamics in table 5.

As a check, C_{ℓ_ϕ} was calculated in a more straightforward manner with the

the digital computer. The computer program consisted of a numerical computation, utilizing the theory presented in reference 8, that resolved the forces on a lifting wing in the presence of a ground plane. The calculation for the same height predicted a smaller value (C_{ℓ_ϕ} = -.02 per radian). However, the

larger value was used in deriving the transfer functions, to be conservative in assessing the influence of ground effect.

Integrated Analysis of the PIO

Linear calculation. - Pilot-in-the-loop, closed loop transfer functions were derived from aircraft transfer functions (listed in table 5) and the system gains. The closed-loop polynomial ratios were then used to predict the dynamic characteristics of the lateral flight control system for inputs below

position and rate saturation. Initial assessments of ground effect were investigated comparatively in this fashion. The linear calculations were also used as a special check case for subsequent nonlinear calculations. However, in deriving the pilot closed-loop response, some generalization is required regarding the feel system because of the nonlinearity associated with commanded roll rate and stick force. For convenience, the outer loop gain is considered to be the pilot gain times the feel gradient.

Figure 9 makes a root locus (pilot closed-loop) comparison of the initial control system implemented on the prototype aircraft in and out of ground effects. The transfer functions for the in-ground-effects case are obtained by including the terms C_{ℓ_ϕ}, C_{n_ϕ}, and C_{y_ϕ}, as presented in the previous section, where bank angle, ϕ, is considered proportional to the difference in height between the right and left wing. A change in height produces a change in lateral moments and accelerations. This, in turn, would be reflected in the lateral transfer functions, as indicated in table 5. The root loci of the two aircraft control system configurations with outer loop closure (K_ϕ increasing) show similar critical gain and frequency characteristics. The equivalent characteristic poles of the lower modes ($\omega_n = 1.25$) with the attitude loop open indicate a lower damping ratio for the aircraft in ground effect, as shown by the dashed slope of figure 9. The same trend is also evident in comparing the two characteristic equations of the basic aircraft in and out of ground effect (table 5). However, this mode ($\omega_n = 1.25$) for both configurations is heavily damped, and any difference thus shown would be unnoticeable by the pilot and not expected to have contributed to the PIO problem.

Nonlinear calculations. - During the PIO, the flight control system was extensively rate and position saturated, as evident in the time history shown in figure 3. Therefore, a realistic analysis requires consideration of these nonlinearities. The discussion that follows in this section utilizes a nonlinear computation of system gain as a function of frequency. This is done by making various amplitude and phase comparisons of four conditions: the initial system on the prototype aircraft and the MFCS both in and out of ground effects. Two pilot inputs are shown for comparison in subsequent figures; $F_a = 4.448$ newtons (1 pound) and $F_a = 35.68$ newtons (8 pounds). The lateral stick force per roll rate varies according to the feel gradient shown in figures 5 and 8.

The method is simply to assign a value to the error vector (amplitude and phase). Then an input/output vector can be determined through each element, keeping track of amplitude and phase algebraically until an open-loop vector is obtained. This makes any vector or vector ratio a function of input and frequency. This procedure is repeated on the digital computer a sufficient number of times to saturate the roll command for the frequency range of interest. For low inputs within the rate and position limits of the system, a linear calculation is used as a computational check.

Appendix B presents details of the nonlinear computational method. The aircraft transfer functions are presented in table 5.

Amplitude and phase plots for the initial aircraft control system, which existed on the prototype aircraft at the time of the first flight, are presented in figures 10(a) and 10(b), respectively. The attenuation is normal with frequency. Higher lateral forces reflect more system gain, due primarily to the nonlinear feel gradient. However, high forces add more phase lag due to rate and position saturation. Above 2.6 radians per second a force input of 35.58 newtons (8 pounds) will rate saturate the system throughout the higher frequency range. Near the PIO frequency ($\omega = 4.0$ rad/sec), the calculations indicate a phase change of -180 degrees.

The initial system in ground effects (figs. 11(a) and 11(b)) in general shows reduction in system gain at the lower frequencies, with little difference evident at the high frequencies. The crossover frequency and critical gain margin are about the same as those shown for the out-of-ground effect configuration.

Figures 12(a) and 12(b) present an amplitude and phase variation, with the frequency of the MFCS configuration in ground effect over the same frequency range as the initial system on the prototype aircraft. The system gain has been reduced sufficiently so that the system behaves in a linear fashion for the two lateral force inputs shown. This is apparent if it is noted that the gain difference between the two force levels is the same and that the phase angle variation is the same throughout the frequency range.

In order to sustain an oscillation in a closed-loop system, the total gain must be unity at a phase shift of -180 degrees (minimum conditions, according to the Nyquist criteria). If it is assumed that the pilot acts as pure gain, with no phase changes, the pilot gain required to cause a PIO would be the gain margin at a -180 degree phase shift. Because of the nonlinearity, the critical pilot gain would also be a function of the lateral stick force input, F_a. Figures 13 and 14 present PIO frequency and critical pilot gain variation as a function of lateral stick force for various control configurations. Low force input approaches the linear values of crossover frequency and gain as predicted by the root locus (fig. 9).

Ground effects, as noted previously (fig. 9), have little effect on the critical pilot gain. For reasonable values of input, the critical pilot gain with the MFCS has been increased by a factor of 4, or at least 10 decibels. This is indicated by the level of the two curves (F_a/ϕ_e) as a function of F_a shown in figure 14. Also, as is evident by the constant value of PIO frequency, the MFCS configuration behaves in a linear fashion throughout the force level presented.

A detailed investigation of the initial control system using the nonlinear calculations indicates that rate saturation exists throughout the higher frequency range (from 2.6 to at least 8 rad/sec) at the highest command response. Total flaperon surface position difference versus input frequency is presented

14

in figure 15 for the initial control system in ground effect. Rate limiting ($A\omega$ = 112 deg/sec) is shown by the hyperbolic boundary. The command response to the flaperon is position limited at the lower frequencies and decreases according to the first order lag of the actuator. As noted, above 2.6 radians per second, flaperon surface is limited in travel by the maximum rate.

A comparison of flaperon surface limitations is presented in figure 16 for the MFCS configuration for three levels of force input. A force input of 35.6 newtons (8 pounds) causes no surface saturation. A force input of 53.4 newtons (12 pounds) will be marginally rate limited at high frequencies. Above 71.2 newtons (16 pounds), maximum roll rate is commanded and the system will rate saturate above 3.5 radians per second; this is below the flaperon surface limit.

CONCLUSIONS

A lateral pilot-induced oscillation (PIO) experienced on the first flight of the YF-16 aircraft was analyzed by linear and nonlinear techniques. In general, the analysis indicates:

(1) The nonlinear technique can be used to analyze this type of control problem. For small inputs, where saturation does not occur, the linear and nonlinear computations agree.

(2) The pilot system phase relationship (bank angle/pilot input) during the PIO was at least -180 degrees. The PIO frequency for out-of-phase response was 3.2 radians per second. Under high pilot gain conditions, the initial flight control system response and control actions could result in a PIO as experienced on the first flight.

(3) The rate command system essentially behaves the same dynamically regardless of the proximity of the ground plane.

(4) Control system modifications (MFCS) for the takeoff and landing phases have increased the pilot gain required to PIO the aircraft by about 10 decibels and also made the mechanical system more difficult to position and rate saturate.

Dryden Flight Research Center
  National Aeronautics and Space Administration
    Edwards, Calif., August 24, 1979

APPENDIX A - GENERAL DYNAMICS FLIGHT REPORT

The first flight of the YF-16 airplane was conducted at Edwards, California by General Dynamics Engineering Test Pilot P. F. Oestricher. The following material is the flight test report in its entirety as submitted by the pilot, and represents a rather complete description regarding the pilot's impression of the PIO experienced during the unintentional lift-off.

"The purpose of these series of tests was to perform a limited functional check of various systems (including the instrumentation system and test control at Bldg. 3940 and the trailer) and to determine the taxi characteristics at various speeds.

"The test configuration was that of the basic airplane with an AIM-9 missile mounted on each wingtip. The airplane was fully fueled at the start of the tests and was ready in all respects.

"Taxiing at normal speeds was evaluated while moving the airplane to the "last chance" check area for runway 22. Periodic application of brakes was required to prevent an excessive speed buildup. The braking effort expended by the pilot (product of pedal force and duration of pedal displacement) was perhaps 30 percent to 50 percent more than required in the case of a fully fueled, clean configured RF-4C. Nose wheel steering was used throughout the run and proved to be precise and easily controlled. Following a check by the mobile crew, the airplane was positioned on runway 22 for an idle power taxi run without brake restraint. A taxi speed of around 30 knots was noted during this test. After a period of straight ahead taxiing, several S-turns were made with no difficulty. The airplane was stopped after traversing about 5,000 feet.

"Following an inspection by the mobile crew, the airplane accelerated toward a target speed of 80 knots. It is believed that an overshoot of about 10 knots occurred on this run. The nose wheel steering appeared to be overly sensitive at speeds of 50 knots or higher and was accordingly disengaged. Directional control by rudder was very satisfactory after the NWS disengagement. The airplane was stopped using moderate brake pedal force after traveling about 5,000 feet. It was then towed back to the "last chance" area for runway 22 for brake cooling.

"The brakes were checked and found to have cooled sufficiently to resume the taxi tests. A normal start was accomplished as were the pre-takeoff check list items. The IIRS was aligned and checked for proper operation. The airplane was positioned on runway 22 for the planned 135 knot high speed taxi run. The brakes were held and the power level slowly advanced to determine the RPM at which wheel slide would occur. This was determined to be about 87% RPM. The gross weight at this time was about 21,200 lbs. The corresponding C.G. was 34.3% M.A.C. The engine was kept at idle RPM until the runway winds (as reported by the tower) dropped below the 12 knot maximum agreed to for the taxi run. Upon tower clearance for the run, the brakes were released and intermediate power selected for a period of about six seconds, after which a substantial

power reduction was made. Nose wheel steering was disengaged at an estimated 50 knots. At about 130 knots (but apparently with the airplane still accelerating somewhat) the airplane was rotated to about 10 degrees and small lateral stick inputs were made in an attempt to get a feel for control response. No response was noted by the pilot (doubtless because the main gear was still restraining the airplane from rolling) and the angle of attack was intentionally increased a small amount. The airplane had continued to accelerate during this time but the pilot was unaware of the fact. Immediately upon rotating the second time, the airplane lifted off with the left wing dropping rather rapidly. Right roll command was applied and the airplane was immediately involved in a fairly high frequency lateral PIO (10 cycles in 14.3 seconds). Eventually, the roll oscillation was stopped but not before lightly touching the rolleron wheel on the lower outboard fin of the left AIM-9 to the runway, striking the right horizontal tail tip (at the trailing edge) on the runway, bouncing off the main landing gear several times in a nose-high and generally symmetrical manner, and developing a substantial heading deviation from the runway axis. The latter factor prompted the decision to fly out of the situation as it was felt that it would be impossible to steer the airplane so as to remain on the runway, even if the nose wheel could be quickly brought down to the surface. Intermediate power was applied for a short period of time after which a fairly low thrust level was held. The airplane was allowed to slowly climb away in a shallow left turn, with a minimum of pilot control inputs being made. A downwind leg to runway 22 was established at about 600 feet AGL at 175 KIAS. The ADC caution light was noted to be on at this time. No attempt was made to turn the light out by resetting. A wide pattern was flown to a long, decelerating final approach with 12 degrees being established just prior to touchdown. A very slight (low amplitude and frequency) lateral motion was noted prior to touchdown. The ground effect was quite pronounced and the engine was brought to idle while still airborne. Aft stick force was relaxed after touchdown and the nose wheel fell gently to the runway, at which time the speed brakes were commanded open. It should be noted that the pitch trim was still in the neutral position at landing since no pilot trim had been applied during the flight. Moderate braking was applied until the airplane was stopped. Following an inspection by the mobile crew, the engine was shut down and the airplane was towed to the hangar.

"The tactics attempted during the PIO are evident from watching the excellent movie films available. Briefly the attempt was to:

1. Keep the wingtips off the runway and stop the roll oscillation with the wings level.

2. Recover the nose high attitude when the lateral control problem had been solved.

3. Control altitude and vertical velocity with thrust. It is believed that this particular attempt was relatively successful.

"No sideslip was noted by the pilot at any time despite the violent nature of the oscillation and the full lateral commands being applied. The roll control problem appeared to be the most serious by far, and accounted for most of

the pilot's attention at the time. Once away from the ground, and the need to keep roll angle within tight bounds, the pilot was able to relax, with the results which are evident in the movie film. The pattern and landing were understandably somewhat conservatire [sic] although a small rudder doublet was performed during the final portion of the approach in an attempt to assess directional control sensitivity. No dibedral [sic] effect was noted and the airplane felt somewhat sensitive as compared to other tactical airplanes.

"Takeoff and landing gross weight/C.G. combinations were 21,100 lbs./34.3% M.A.C. and 20,300 lbs./35.0 % M.A.C., respectively."

APPENDIX B - BASIC NONLINEAR ANALYSIS AND COMPUTATIONAL PROCEDURE

Nonlinear Analysis

The functional block diagram shown in figure 17 is used for total lateral control system nonlinear definition and analysis. Each and all forward, feedback and common paths are as indicated or represented equivalently. The initial task is to further separate the common paths through the rudder loop so that the overall mathematical description of the open-loop attitude system will contain only one summation junction. This finalized description will then enable an explicit solution for the input by adding the roll rate feedback ($K_p p$) to the error signal commanded ($\dot{\phi}_e$).

From the figure 17, the following set of equations are evident.

$$\delta_r = \left(H_y A_y + H_r r - H_p p + \dot{\phi}_e \right) G_r$$

$$A_y = \left(G_H \frac{A_y}{\delta_a} + G_F \frac{A_y}{\delta_F} \right) \dot{\phi}_e + \frac{A_y}{\delta_r} \delta_r$$

$$r = \left(G_H \frac{r}{\delta_a} + G_F \frac{r}{\delta_F} \right) \dot{\phi}_e + \frac{r}{\delta_r} \delta_r$$

$$p = \left(G_H \frac{p}{\delta_a} + G_F \frac{p}{\delta_F} \right) \dot{\phi}_e + \frac{p}{\delta_r} \delta_r$$

where

$$\delta_a = G_H \dot{\phi}_e$$

and

$$\delta_F = G_F \dot{\phi}_e$$

The nonlinearities are appropriately included in subsequent numerical computations. Substituting A_y, r, and p into the δ_r equation and rearranging gives:

$$\frac{\delta_r}{\dot{\phi}_e} = \frac{G_r\left(1 + H_yG_H\frac{A_y}{\delta_a} + H_yG_F\frac{A_y}{\delta_F} + H_rG_H\frac{r}{\delta_a} + H_rG_F\frac{r}{\delta_F} - H_pG_H\frac{p}{\delta_a} - H_pG_F\frac{p}{\delta_F}\right)}{H(s)} \tag{1}$$

where

$$H(s) = 1 - H_yG_r\frac{A_y}{\delta_r} - H_rG_r\frac{r}{\delta_r} + H_pG_r\frac{p}{\delta_r} \tag{2}$$

The total roll rate commanded per error signal $\dot{\phi}_e$ is:

$$\frac{p}{\dot{\phi}_e} = G_H\frac{p}{\delta_a} + G_F\frac{p}{\delta_F} + \frac{p}{\delta_r}\frac{\delta_r}{\dot{\phi}_e} \tag{3}$$

or

$$\frac{p}{\dot{\phi}_e} = \frac{G_H\frac{p}{\delta_a} + G_F\frac{p}{\delta_a}}{H(s)} H(s) + \frac{p}{\delta_r}\frac{\delta_r}{\dot{\phi}_e} \tag{4}$$

Substituting $H(s)$ and $\dfrac{\delta_r}{\dot{\phi}_e}$ into the above equation, and then multiplying through,

canceling and regrouping the aircraft transfer functions with respect to roll response yields:

$$\frac{p}{\dot{\phi}_e} = \frac{\left(G_H\frac{p}{\delta_a} + G_F\frac{p}{\delta_F}\right)\left(1 - H_yG_r\frac{A_y}{\delta_r} - H_rG_r\frac{r}{\delta_r}\right) + G_r\frac{p}{\delta_r}\left[1 + H_y\left(G_H\frac{A_y}{\delta_a} + G_F\frac{A_y}{\delta_F}\right) + H_r\left(G_H\frac{r}{\delta_a} + G_F\frac{r}{\delta_F}\right)\right]}{H(s)} \tag{5}$$

Since no nonlinearities are present in the rudder closed-loop feedback function $H(s)$, this function in subsequent computations can be conveniently

20

moved downstream to the roll rate and roll attitude loops as $\frac{1}{H(s)}$ and

$\frac{1}{s\ H(s)}$, respectively. The aircraft open-loop transfer functions are listed in table 5. The actuator transfer functions G_H, G_F, and G_r (including their effective gains) and the feedback functions H_y, H_r, and H_p are as follows:

$$G_H = \frac{5}{s + 20} \qquad\qquad H_y = .296$$

$$G_F = \frac{20}{s + 20} \qquad\qquad H_r = \frac{1.33\ (3s + 15)s}{(s + 15)\ (s + 1)}$$

$$G_r = \frac{11.25}{s + 20} \qquad\qquad H_p = \frac{.345\ (3s + 15)s}{(s + 15)\ (s + 1)}$$

In order to list and define the flaperon rate and position limit boundary in computing the total roll response, equation (5) is separated so as to reflect the output of each individual surface.

$$\frac{\dot{p}}{\phi_{e}}_{(aileron)} = G_H\ \frac{p}{\delta_a}\left(1 - H_y G_r\ \frac{A_y}{\delta_r} - H_r G_r\ \frac{r}{\delta_r}\right) \qquad (6)$$

$$\frac{\dot{p}}{\phi_{e}}_{(flaperon)} = G_F\ \frac{p}{\delta_F}\left(1 - H_y G_r\ \frac{A_y}{\delta_r} - H_r G_r\ \frac{r}{\delta_r}\right) \qquad (7)$$

$$\frac{\dot{p}}{\phi_{e}}_{(rudder)} = G_r\ \frac{p}{\delta_r}\left[1 + H_y\left(G_H\ \frac{A_y}{\delta_a} + G_F\ \frac{A_y}{\delta_r}\right) + H_r\left(G_H\ \frac{r}{\delta_a} + G_F\ \frac{r}{\delta_F}\right)\right] \qquad (8)$$

The roll contribution is small due to A_y and r in the above rudder equation (eq. (8)). However, for the sake of completeness, all terms are included in subsequent computations.

Computational Procedure

The flow diagram shown in figure 18 represents the YF-16 aircraft roll control system, aerodynamics, and equivalent rudder interconnect and feedback loops.

In the diagram, T1 represents the pilot as a pure gain constant. Thus, the commanded input X_3 is proportional to the error in bank angle X_2 ($X_2 = \phi_R - \phi_{A/C}$). Also, the output of any quantity X_4, X_5, and so forth depends on X_2 and the intermediate transfer function T2 and T3. T2 is the transfer function for each of the feel systems shown in figures 5 and 7. For both system configurations, T3 is the forward loop model $\frac{10}{s + 10}$ of the dual lag system.

As previously shown, it was convenient to rearrange the rudder interconnect loops such that the functions T9, T13, T16, T17, and T18 gave an equivalent representation for the separated loops. The aerodynamic transfer functions for both in and out of ground effects are listed in table 5. In order to express the subsequent rate limit T11 as the total difference between the two surfaces, the gain constant of T13 is equal to half the listed value. This representation can be used for both linear and nonlinear calculations. However, for nonlinear calculations the input/output ratio, both amplitude and phase, will be a function of the input.

To obtain a frequency response, various values are assumed and assigned to X_6 (A, ω), a vector that is a function of both frequency and amplitude.

Then the vector signal is traced for each calculation. The phase and amplitude of each successive vector are noted through each block and summation junction until an input/output vector relationship is determined.

The logic, vector algebra, and transfer functions shown in table 6 for various configurations were programmed on a digital computer. In the equations, $s = j\omega$, where ω is a variable, and X_6 is a variable.

REFERENCES

1. Ashkenas, Irving L.; Jex, Henry R.; and McRuer, Duane T.: Pilot-Induced Oscillations: Their Cause and Analysis. STI TR-239-2, Systems Technology, Inc., June 20, 1964.

2. Smith, John W.; and Berry, Donald T.: Analysis of Longitudinal Pilot-Induced Oscillations Tendencies of YF-12 Aircraft. NASA TND-7900, 1975.

3. Eggers, James A.; and Bryant, William F., Jr.: Flying Qualities Evaluation of the YF-16 Prototype Lightweight Fighter. AFFTC-75-15, Air Force Flight Test Center, Edwards AFB, July 1975.

4. Mechtly, E. A.: The International System of Units - Physical Constants and Conversion Factors. Second Revision. NASA SP-7012, 1973.

5. Stability and Flight Control. Flight Control System Description. FZM-401-035, General Dynamics, Convair Aerospace Div., Nov. 1, 1972.

6. Stability and Flight Control. Aerodynamics Data Summary. Vol. I - Rigid Wind Tunnel Data. FZM-401-041 Rev. B, General Dynamics, Convair Aerospace Div., Aug. 10, 1973.

7. Anon.: USAF Stability and Control Datcom. Air Force Flight Dynamics Lab., Wright-Patterson Air Force Base, Oct. 1960 (rev. Aug. 1968).

8. Bradley, R. G.; and Miller, B. D.: Application of Finite-Element Theory to Airplane Configurations. AIAA J. Aircraft, vol. 8, no. 6, Am. Inst. Aeronaut. & Astronaut., June 1971, pp. 400-405.

TABLE 1. - PHYSICAL GEOMETRY AND AIRCRAFT CONFIGURATION

$$s = 26.0129 \text{ m}^2 \ (280 \text{ ft}^2)$$

$$\bar{c} = 3.334 \text{ m} \ (10.937 \text{ ft})$$

$$b = 8.891 \text{ m} \ (29.17 \text{ ft})$$

$$w = 9616.157 \text{ kg} \ (21,200 \text{ lb})$$

$$c.g. = 34.3 \text{ percent}$$

$$I_x = 12472.57 \text{ kg-m}^2 \ (92,200 \text{ slug-ft}^2)$$

$$I_z = 78631.43 \text{ kg-m}^2 \ (58,000 \text{ slug-ft}^2)$$

$$I_{xz} = 203.36 \text{ kg-m}^2 \ (150 \text{ slug-ft}^2)$$

TABLE 2. - YF-16 FLIGHT CONTROL LIMITS

(a) Control surfaces

	Authority limits	Rate limits
Horizontal tail	±25 degrees	60 deg/sec
Flaperon	±20 degrees	56 deg/sec
Rudder	±30 degrees	120 deg/sec

(b) Command servos (in series)

	Second order characteristics	
Horizontal tail	$\zeta = .7$ & $\omega_n = 52$	175 deg/sec
Flaperon	$\zeta = .7$ & $\omega_n = 52$	150 deg/sec
Rudder	$\zeta = .7$ & $\omega_n = 52$	210 deg/sec

(c) Secondary surfaces

	Authority limits
Leading edge flaps	0 -------- 30 deg
Trailing edge flaps	0 -------- 20 deg
Speed brakes	0 -------- 60 deg

TABLE 3. - FLIGHT CONDITIONS

$$\alpha = 15°$$
$$M = .20$$
$$h_p = 694.94 \text{ m } (2280 \text{ ft})$$
$$\bar{q} = 2614.248 \text{ N/m}^2 \ (54.60 \text{ lb/ft}^2)$$
$$LEF = 25°$$
$$\text{T.E. flaperon (roll control)} \leq \pm 20°$$
$$V = 67.57 \text{ m/sec } (221.7 \text{ ft/sec})$$
$$\theta_0 = 15°$$

TABLE 4. - REVIEW OF RELEVANT PIO CONDITIONS

(a) First flight of YF-16

1. Frequency = 4.2 rad/sec, .668 hz
2. 12 complete cycles
3. Command input ≈ 160 percent of saturation
4. Total lag between pilot force input and bank angle output $\geq$ 180°
5. Flaperon rate limit = 112 deg/sec (= 2x surface rate)
6. Horizontal tail rate - less than system rate saturation

(b) Conditions common to PIO problems

1. -180° pilot and system relationship
2. Reasonable frequency range
3. Rate limiting

(c) Differences from other aircraft with PIO problems

1. Minimum displacement force stick
2. Ground effect (takeoff)
3. Fly-by-wire (no mechanical overlapping loop) - consequently no "stick talk"
4. High reponse roll command (design requirement)

TABLE 5. - AERODYNAMICS

(a) Body axis stability coefficients

$$C_{\ell_\beta} = -.00508 \qquad\qquad C_{\ell_{\delta_a}} = -.001$$

$$C_{n_\beta} = .0035 \qquad\qquad C_{n_{\delta_a}} = -.00027$$

$$C_{y_\beta} = -.019 \qquad\qquad C_{y_{\delta_a}} = 0.$$

$$C_{\ell_p} = -.205 \qquad\qquad C_{\ell_{\delta_F}} = -.0023$$

$$C_{n_p} = -.08 \qquad\qquad C_{n_{\delta_F}} = -.00024$$

$$C_{y_p} = .21 \qquad\qquad C_{y_{\delta_F}} = 0.$$

$$C_{\ell_r} = .198 \qquad\qquad C_{\ell_{\delta_r}} = .00047$$

$$C_{n_r} = -.54 \qquad\qquad C_{n_{\delta_r}} = -.00173$$

$$C_{y_r} = .9 \qquad\qquad C_{y_{\delta_r}} = .00278$$

TABLE 5 - Continued

(b) Transfer functions – no ground effect

$$\frac{p}{\delta_a} = \frac{-2.77(s - .038)(s + .225 \pm j1.438)^2}{\Delta}$$

$$\frac{p}{\delta_F} = \frac{-6.35(s - .038)(s + .217 \pm j1.308)^2}{\Delta}$$

$$\frac{p}{\delta_r} = \frac{1.29(s - .039)(s - 2.63)(s + 2.50)^2}{\Delta}$$

$$\frac{r}{\delta_a} = \frac{-.126(s + .528)(s - .344 \pm j3.52)^2}{\Delta}$$

$$\frac{r}{\delta_F} = \frac{-.122(s + .524)(s - .976 \pm j4.88)^2}{\Delta}$$

$$\frac{r}{\delta_r} = \frac{-.757(s + .559)(s + .122 \pm j1.69)^2}{\Delta}$$

$$\frac{a_y}{\delta_a} = \frac{-.049(s - 1.266)(s + .384)(s + .357 \pm j1.90)^2}{\Delta}$$

$$\frac{a_y}{\delta_F} = \frac{-.047(s - 3.233)(s + .328)(s + .730 \pm j1.80)^2}{\Delta}$$

$$\frac{a_y}{\delta_r} = \frac{-.180(s - .108)(s + .567)(s + .136 \pm j2.48)^2}{\Delta}$$

where

$$\Delta = (s + .719)(s + .093)(s + .114 \pm j2.27)^2$$

TABLE 5. - Concluded

(c) Additional terms to include ground effects

$$C_{\ell_\phi} = -.0260$$

$$C_{n_\phi} = .00635$$

$$C_{y_\phi} = 1.376$$

(d) Transfer functions including ground effects

$$\frac{p}{\delta_a} = \frac{-2.77(s - .409)(s + .227 \pm j1.428)^2}{\Delta}$$

$$\frac{p}{\delta_F} = \frac{-6.35(s - .0404)(s + .218 \pm j1.301)^2}{\Delta}$$

$$\frac{p}{\delta_r} = \frac{1.29(s - .043)(s - 2.59)(s + 2.47)^2}{\Delta}$$

$$\frac{r}{\delta_a} = \frac{-.126(s + .478)(s - .319 \pm j3.82)^2}{\Delta}$$

$$\frac{r}{\delta_F} = \frac{-.122(s + .485)(s - .957 \pm j5.23)^2}{\Delta}$$

$$\frac{r}{\delta_r} = \frac{-.757(s + .436)(s + .184 \pm j2.00)^2}{\Delta}$$

$$\frac{a_y}{\delta_a} = \frac{-.049(s - .297 \pm j1.008)^2(s + .214 \pm j2.33)^2}{\Delta}$$

$$\frac{a_y}{\delta_F} = \frac{-.047(s - 1.11 \pm j.736)^2(s + .390 \pm j2.31)^2}{\Delta}$$

$$\frac{a_y}{\delta_r} = \frac{-.180(s + .210 \pm j.770)^2(s + .155 \pm j2.53)^2}{\Delta}$$

where

$$\Delta = (s + .373 \pm j.366)^2(s + .144 \pm j2.48)^2$$

TABLE 6. - TRANSFER FUNCTION DEFINITIONS

(a) YF-16 prototype aircraft

Transfer function	Transform (fig. 18)
T1	$X3 = X2*1$
T2	$X4 = .008726(X3)^3 + .06980803(X3)$
	If $|X4| > 3.5$, $X4 = (3.5/|X4|)*X4$
T3	$X5 = (10/(s + 10))*X4$
T4	$X7 = X6*.2$
T5	$X8 = .25*X7$
T6	$X9 = ((20*s)/(s + 20))*X8$
T7	$X10 = X9*1$
	If $|X10| > .934$, $X10 = (.934/|X10|)*X10$
T8	$X11 = X10/s$
T9	$X12 = \frac{p}{\delta_a}*\left(1 - H_yG_r\frac{A_y}{\delta_r} - H_rG_r\frac{r}{\delta_r}\right)*X11$
T10	$X13 = ((20*s)/(s + 20))*X7$
T11	$X14 = X13*2$
	If $|X14| > 1.868$, $X14 = (1.868/|X14|)*X14$
T12	$X15 = X14/s$
	If $|X15| > .698$, $X15 = (.698/|X15|)*X15$
T13	$X16 = \frac{1}{2}*\frac{p}{\delta_F}*\left(1 - H_yG_r\frac{A_y}{\delta_r} - H_rG_r\frac{r}{\delta_r}\right)*X15$
T14	$X17 = .563*X7$
T15	$X18 = (20/(s + 20))*X17$
T16	$X19 = \frac{p}{\delta_r}*\left[1 + H_y\left(G_H\frac{A_y}{\delta_a} + G_F\frac{A_y}{\delta_r}\right) + H_r\left(G_H\frac{r}{\delta_a} + G_F\frac{r}{\delta_F}\right)\right]*X18$
T17	$X21 = \dfrac{1}{1 - H_yG_r\frac{A_y}{\delta_r} - H_rG_r\frac{r}{\delta_r} + H_rG_r\frac{p}{\delta_r}}*X20$
T18	$X22 = \dfrac{1}{s\left(1 - H_yG_r\frac{A_y}{\delta_r} - H_rG_r\frac{r}{\delta_r} + H_rG_r\frac{p}{\delta_r}\right)}*X20$

(b) Modified flight control system

Prototype control system		MFCS
Change T2	to	$X4 = .0007487(X3)^3 + .01745(X3)$
		$|X4| \leq 2.91$
T4		$X7 = X6*.12$

Leading edge flap

δ_F (flaperon)

δ_a (horizontal tail)

Speed brakes

8.89 m
29.17 ft

4.95 m
16.25 ft

δ_R (rudder)

14.17 m
46.50 ft
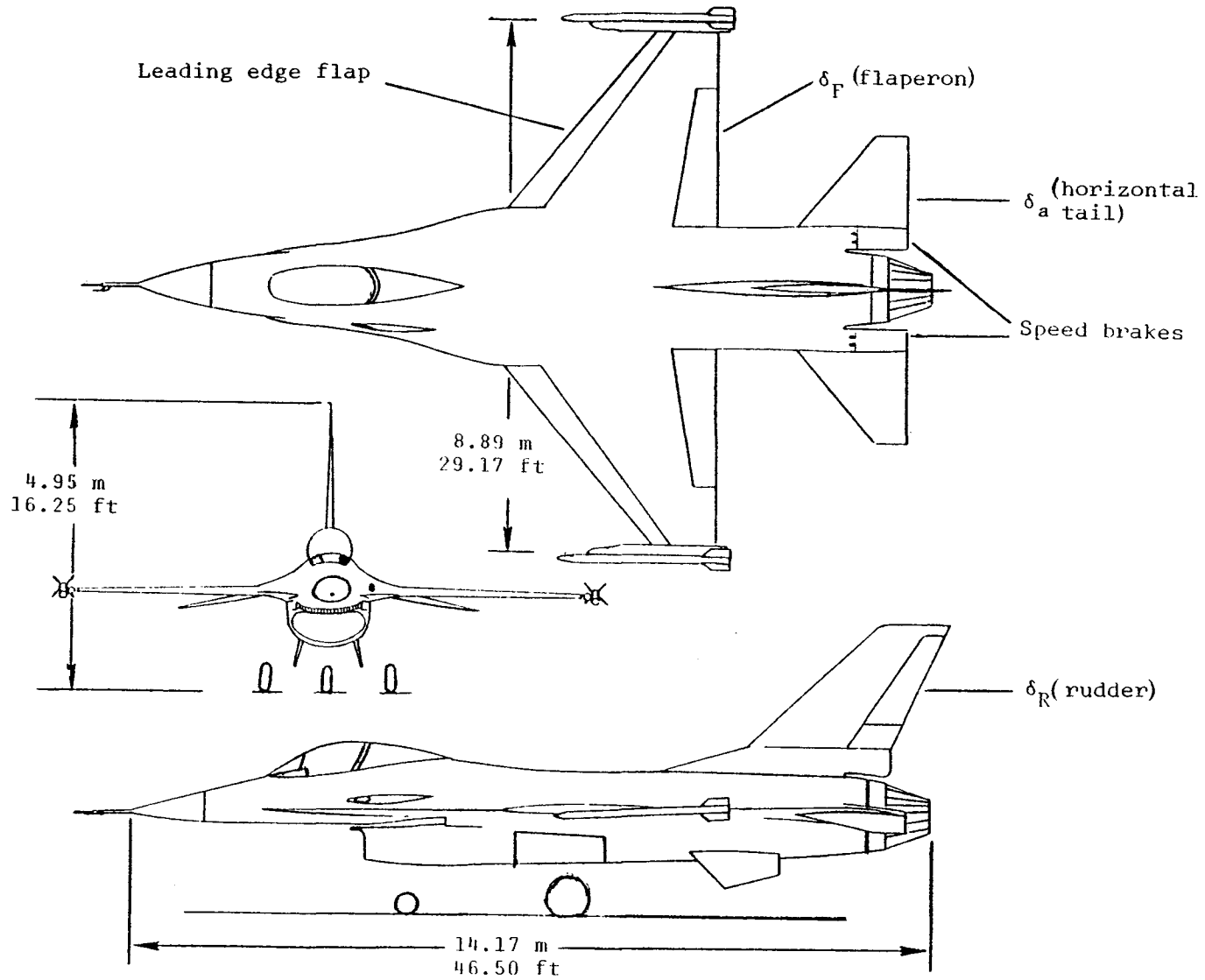
Figure 1. YF-16 primary control surfaces.
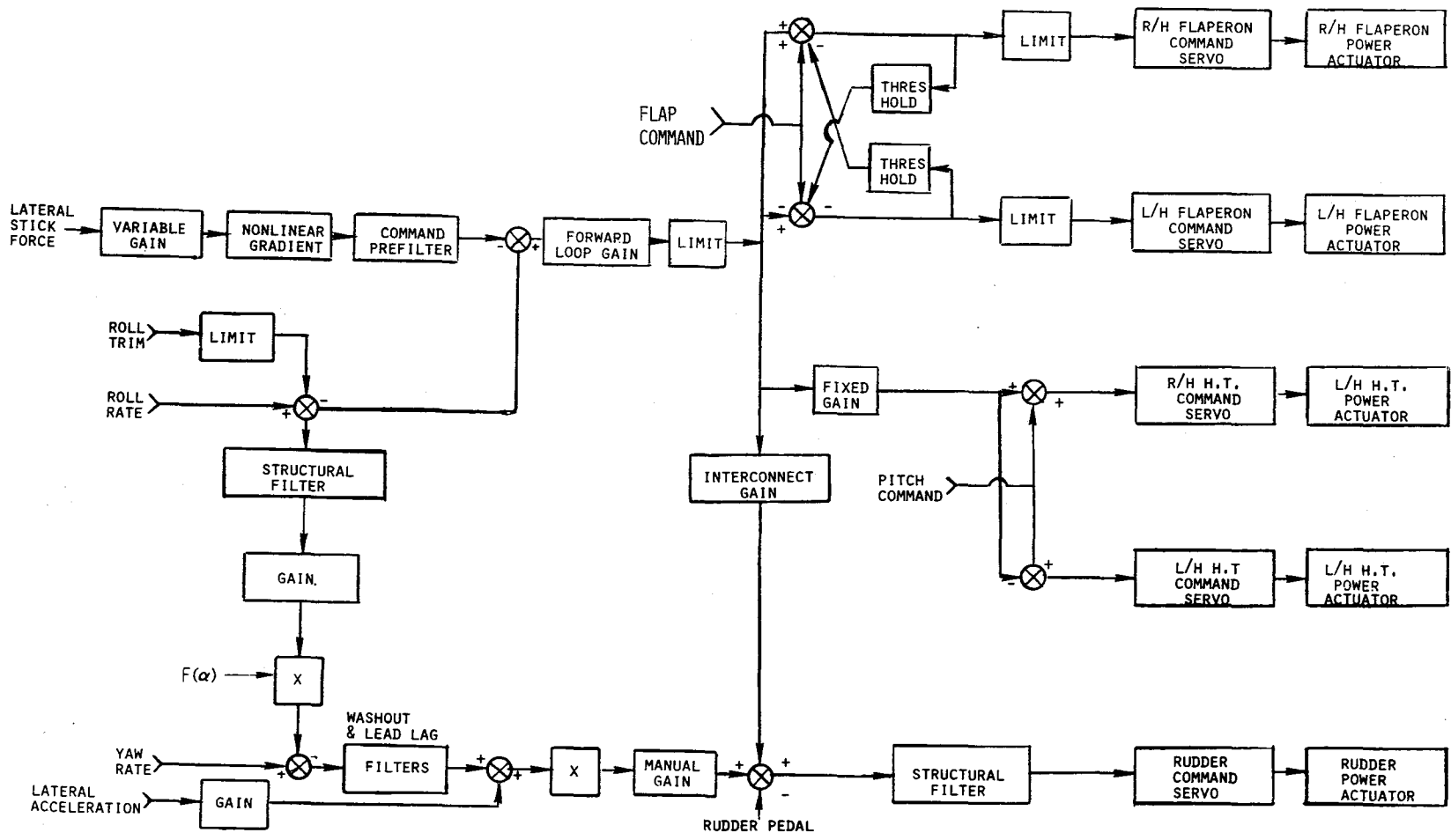
Figure 2. Simplified roll and yaw axis flight control system.

RT

F_a, N
60
0
-60

15
0
-15
F_a, lb

TED

$\delta_{HT/L}$, deg
30
0
-30

TED

$\delta_{HT/R}$, deg
30
0
-30

TED

$\delta_{F/L}$, deg
20
0
-20

TED

$\delta_{F/R}$, deg
20
0
-20

δ_r, deg
20
0
-20

LIFT-OFF

p, deg/sec
200
0
-200

0   10   20

t , sec
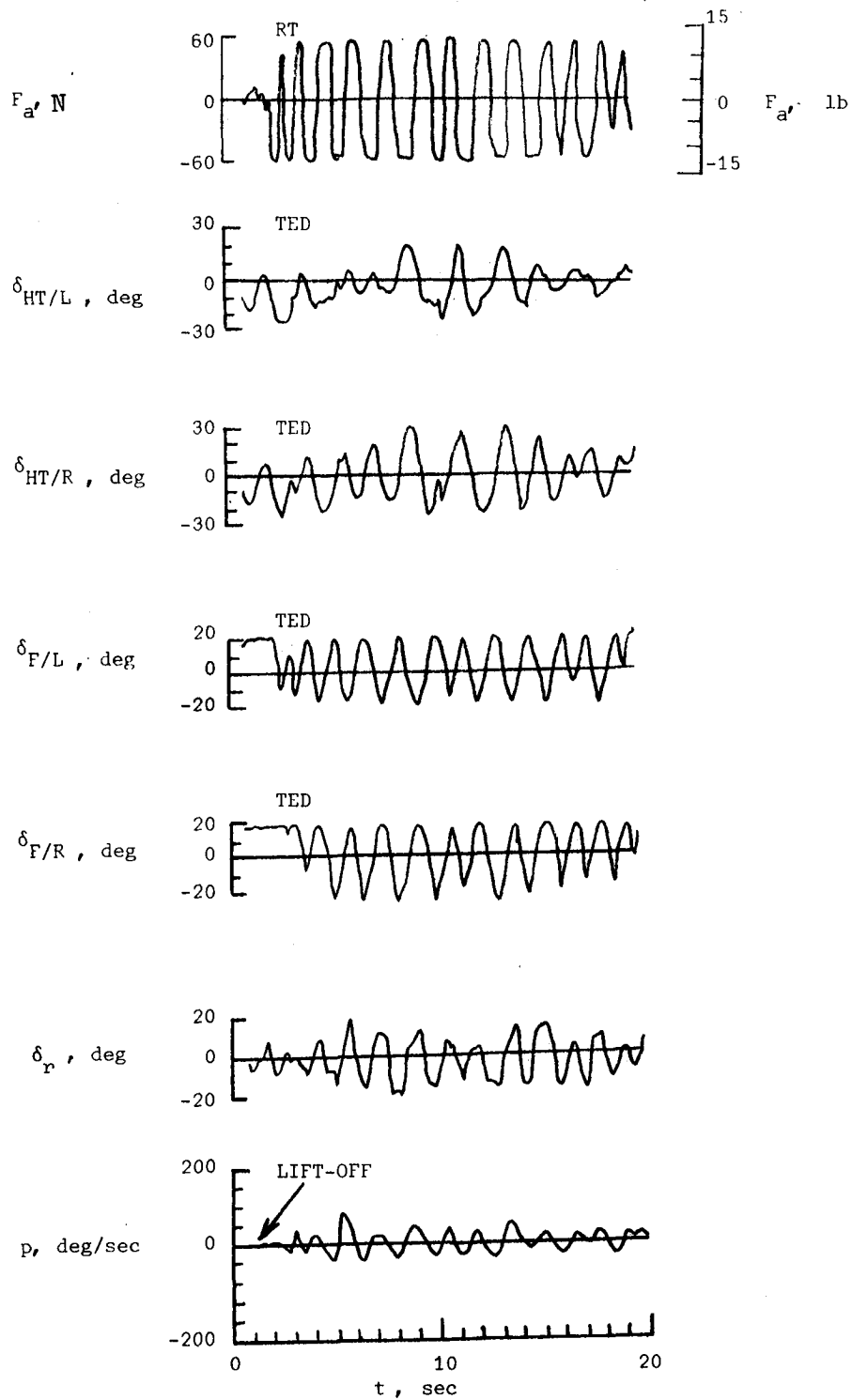
Figure 3. YF-16 pilot induced oscillation ex-
perienced on the first flight.

AIRCRAFT
TRANSFER FUNCTION

ACTUATORS

K A_H δ_a

HORIZONTAL TAIL

STICK FORCE
GRADIENT

PILOT GAIN

COMMAND
PREFILTER

ϕ_R + ϕ_e $\frac{F_s}{\phi}$ $\frac{\dot{\phi}_c}{F_s}$ N(s) $-$ +   KN

δ_F

A_H

FLAPERON

ϕ

p

A/C

r

SCHEDULED
GAIN

AILERON
- RUDDER
INTERCONNECT

$\phi_{A/C}$ (AIRCRAFT ATTITUDE)

K_p

+   RUDDER A_H δ_r

A_y

+   K

ROLL RATE
FEEDBACK

+   FILTERS   YAW, ROLL
- RUDDER INTERCONNECT

+

$-$ SCHEDULED
GAIN

Figure 4. Conceptual block diagram of lateral control elements.
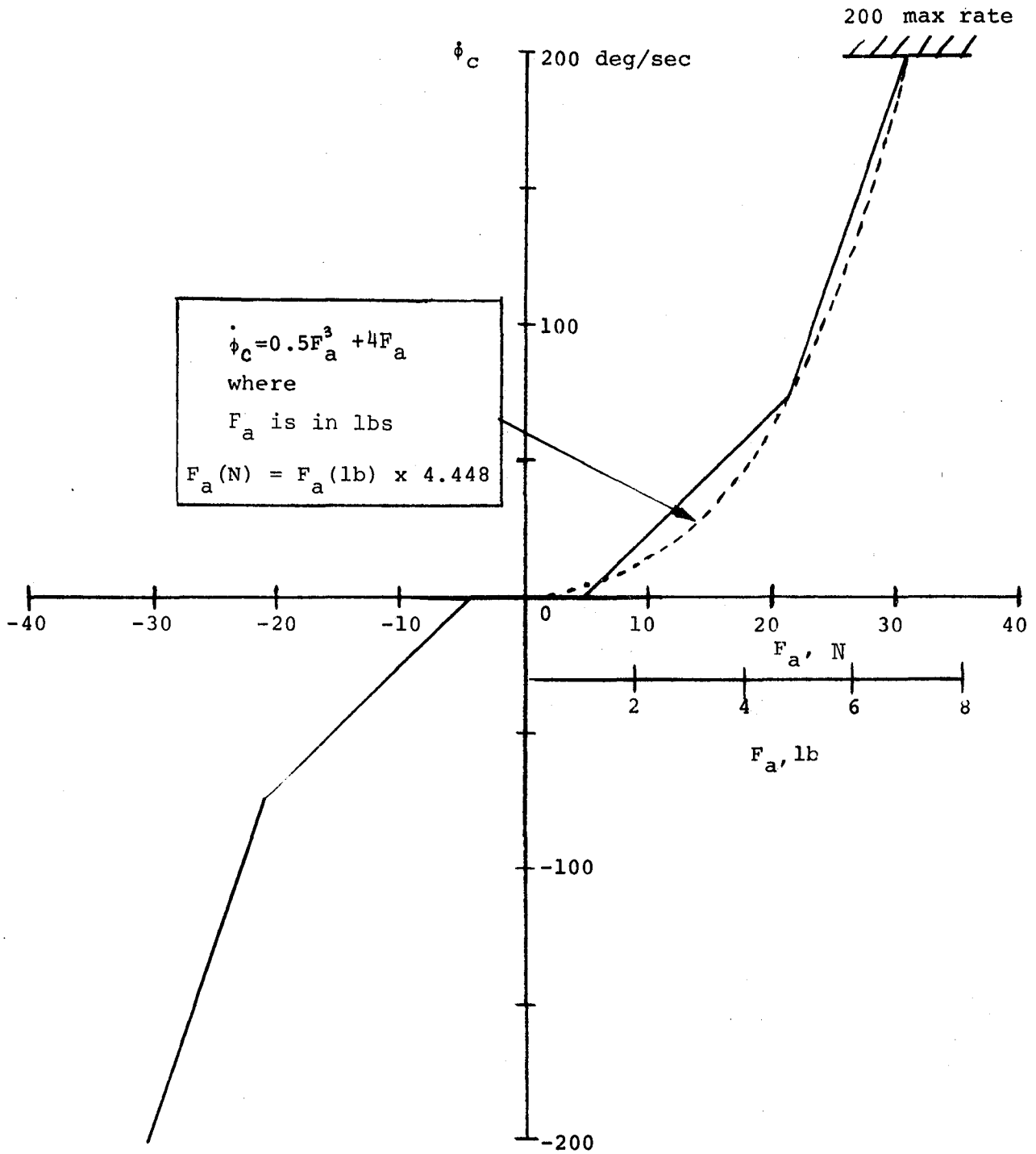
Figure 5.   Initial roll command gradient on the prototype aircraft.
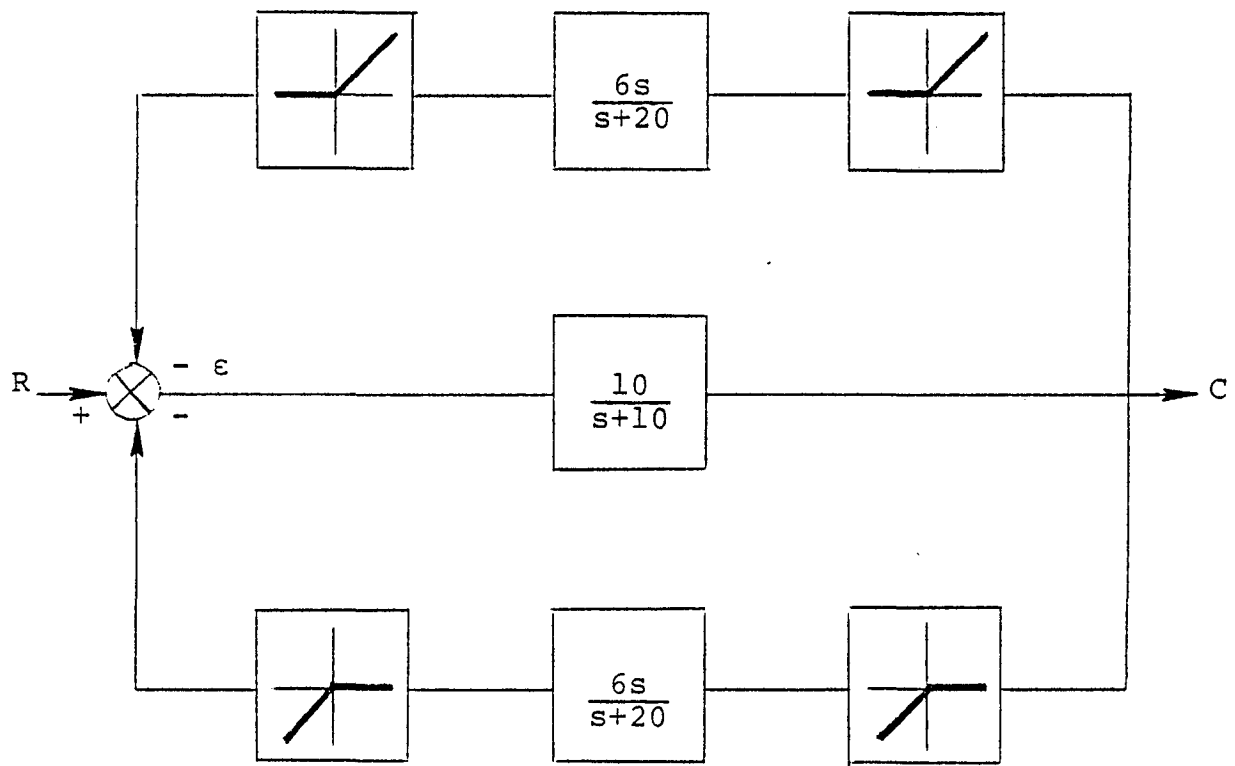
Figure 6. Block diagram of the FY-16 dual lag system (command prefilter).
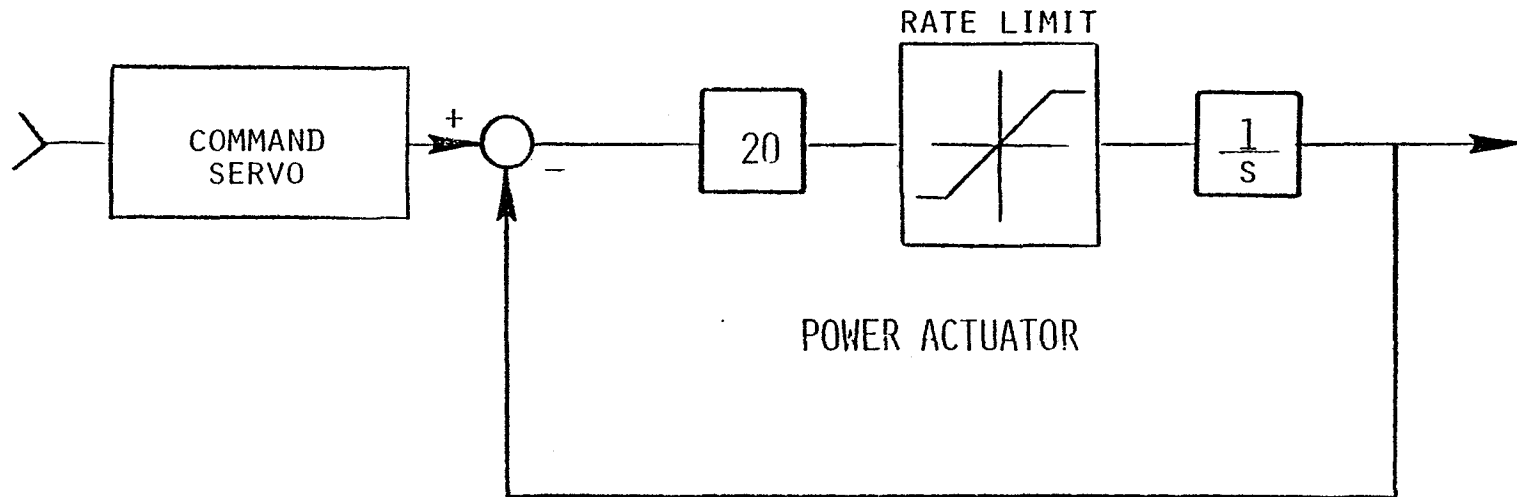
Figure 7. Diagram description of the horizontal tail, flaperon, and rudder mechanical system.
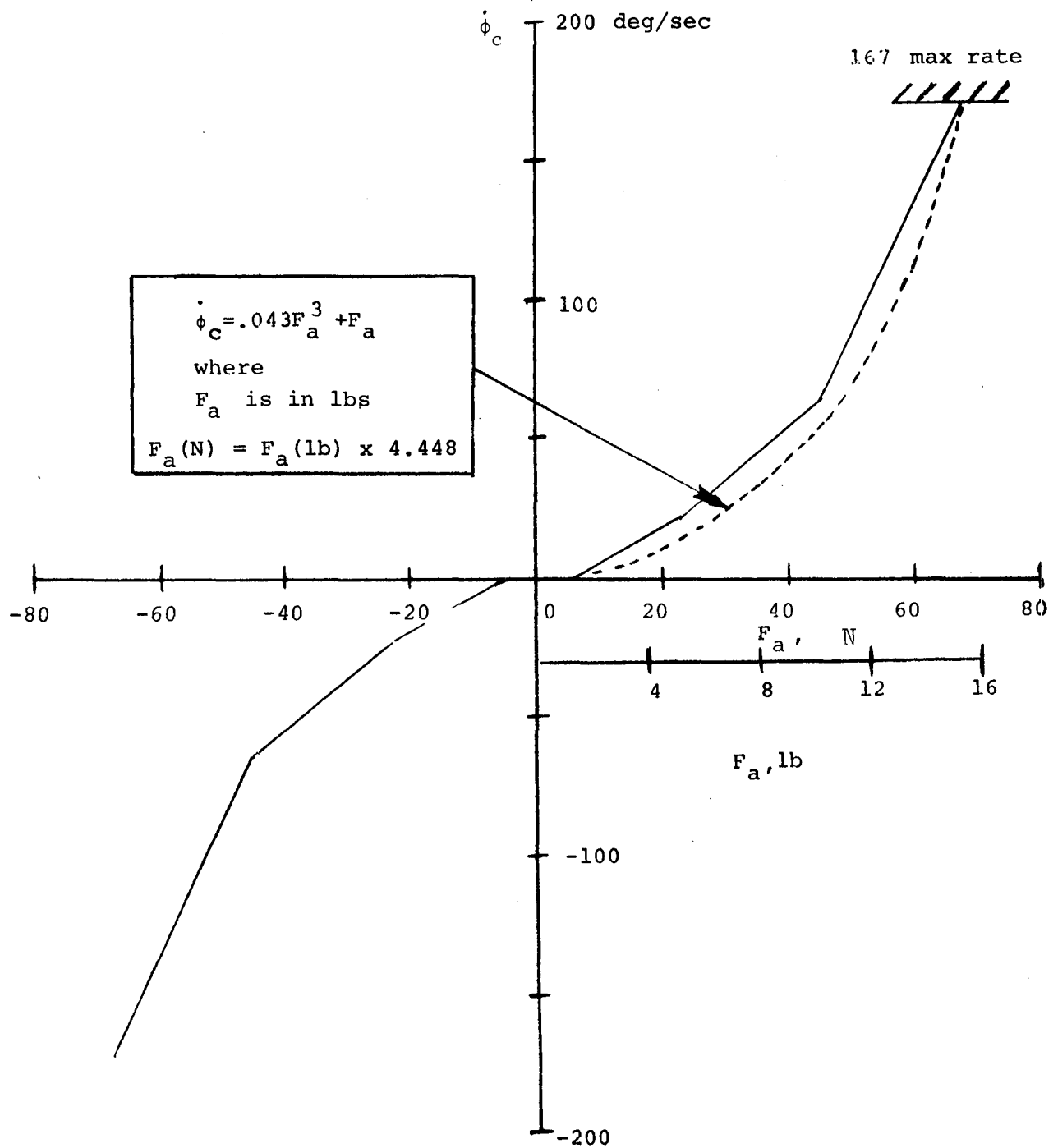
Figure 8. YF-16 roll command gradient (MFCS).

$$\dot{\phi}_c = .043 F_a^3 + F_a$$

where
F_a is in lbs

$$F_a(N) = F_a(lb) \times 4.448$$

ω_c = 4.1 rad/sec

K_{ϕ_c} = 13

jω, rad/sec

§ = .9

σ, rad/sec

(b) In ground effects.

ω_c = 3.9 rad/sec

K_{ϕ_c} = 13

jω, rad/sec

§ = .9

σ, rad/sec
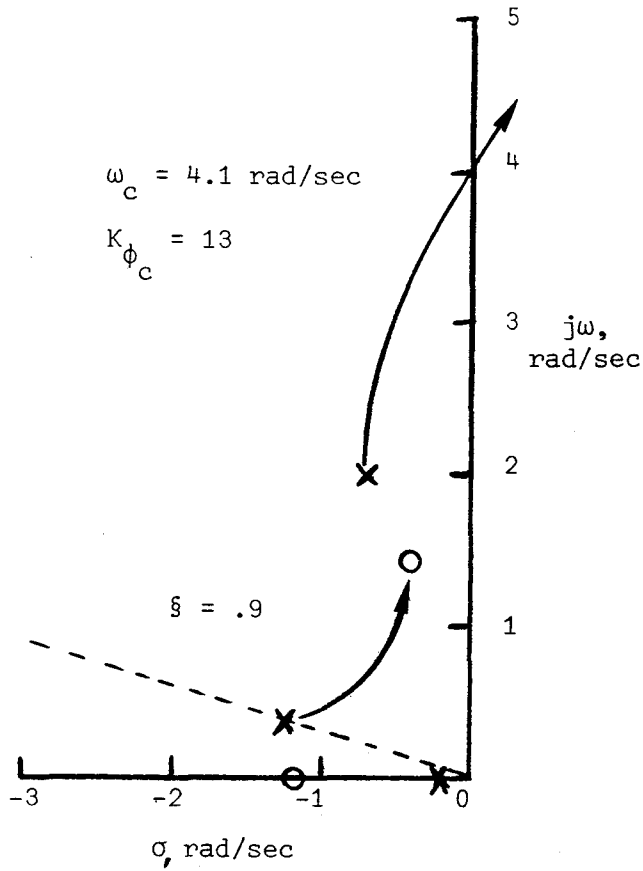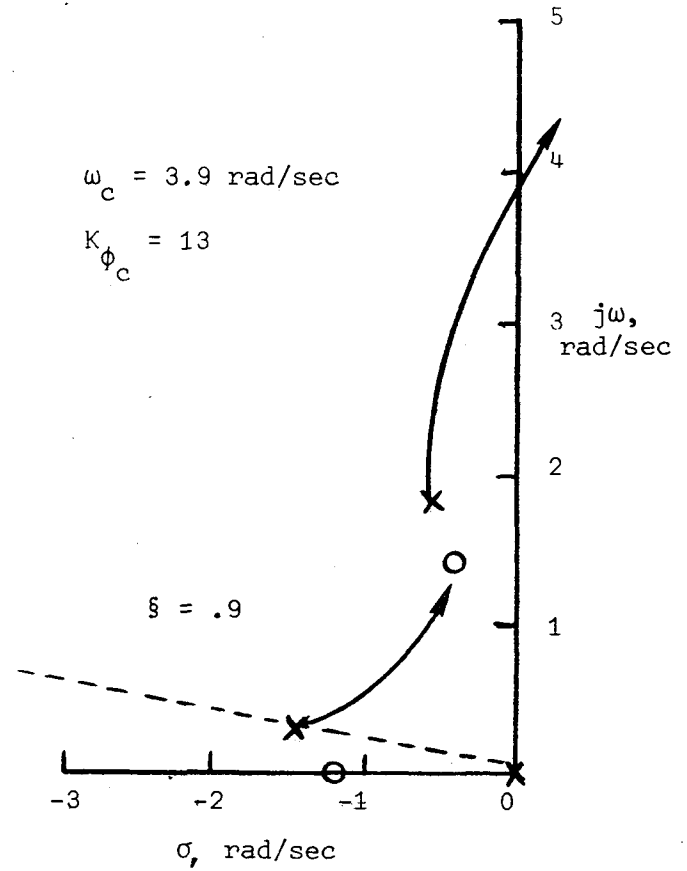
(a) Out of ground effects.

Figure 9. Root locus of altitude loop for the initial control system on the prototype aircraft.
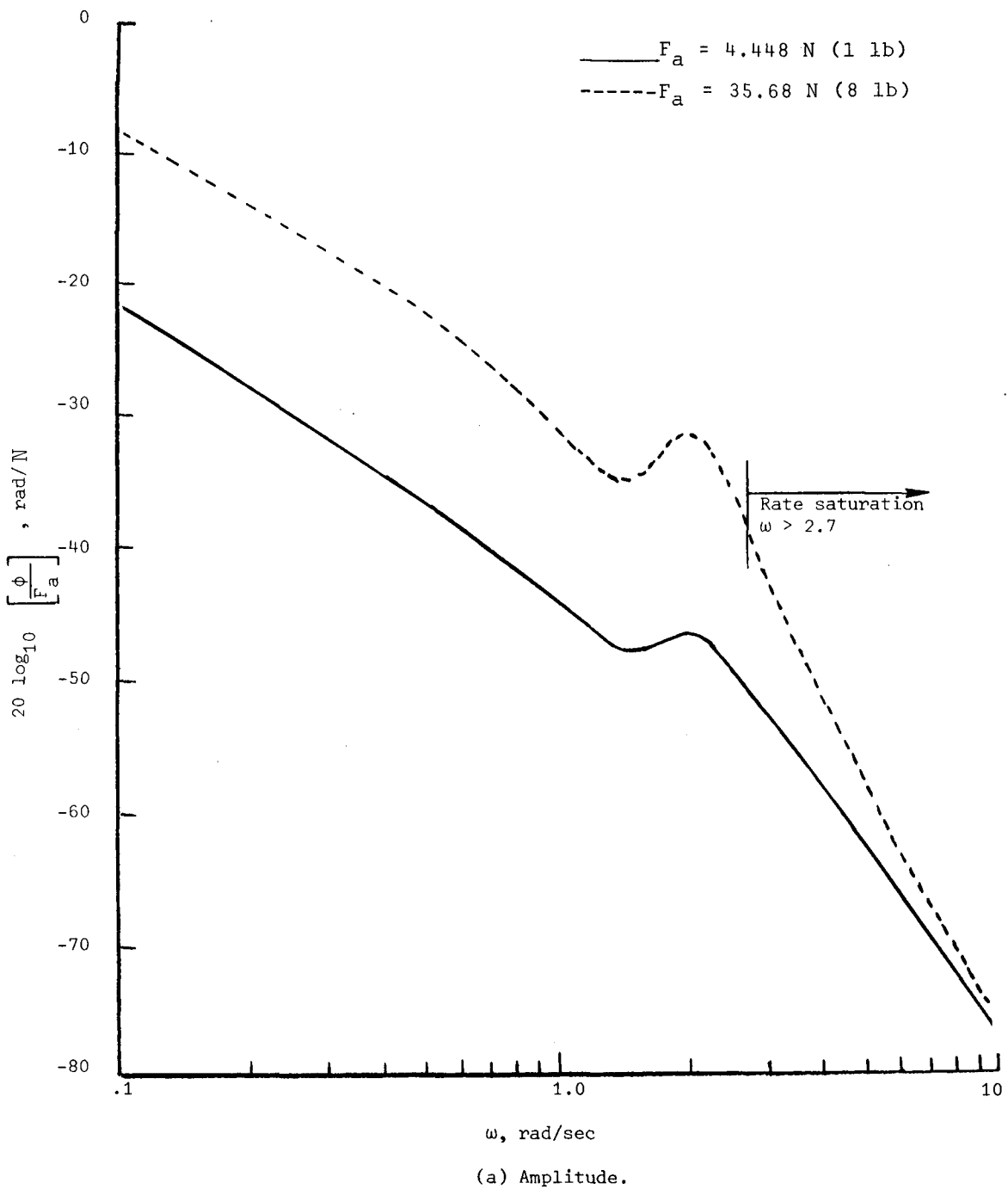
Figure 10. Frequency response of initial control system, out of ground effects, with pilot loop open.
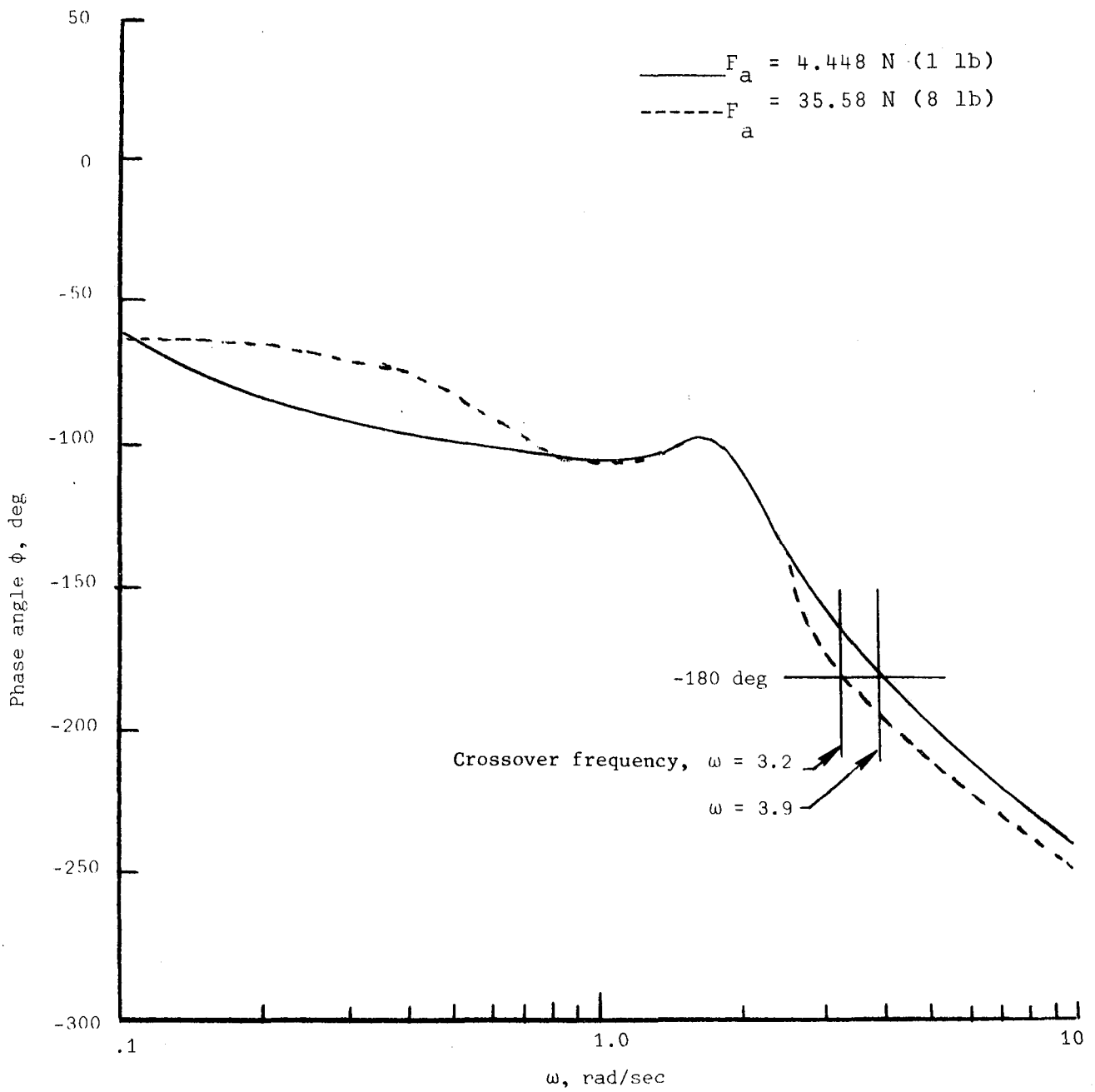
(b) Phase angle.

Figure 10. Concluded.
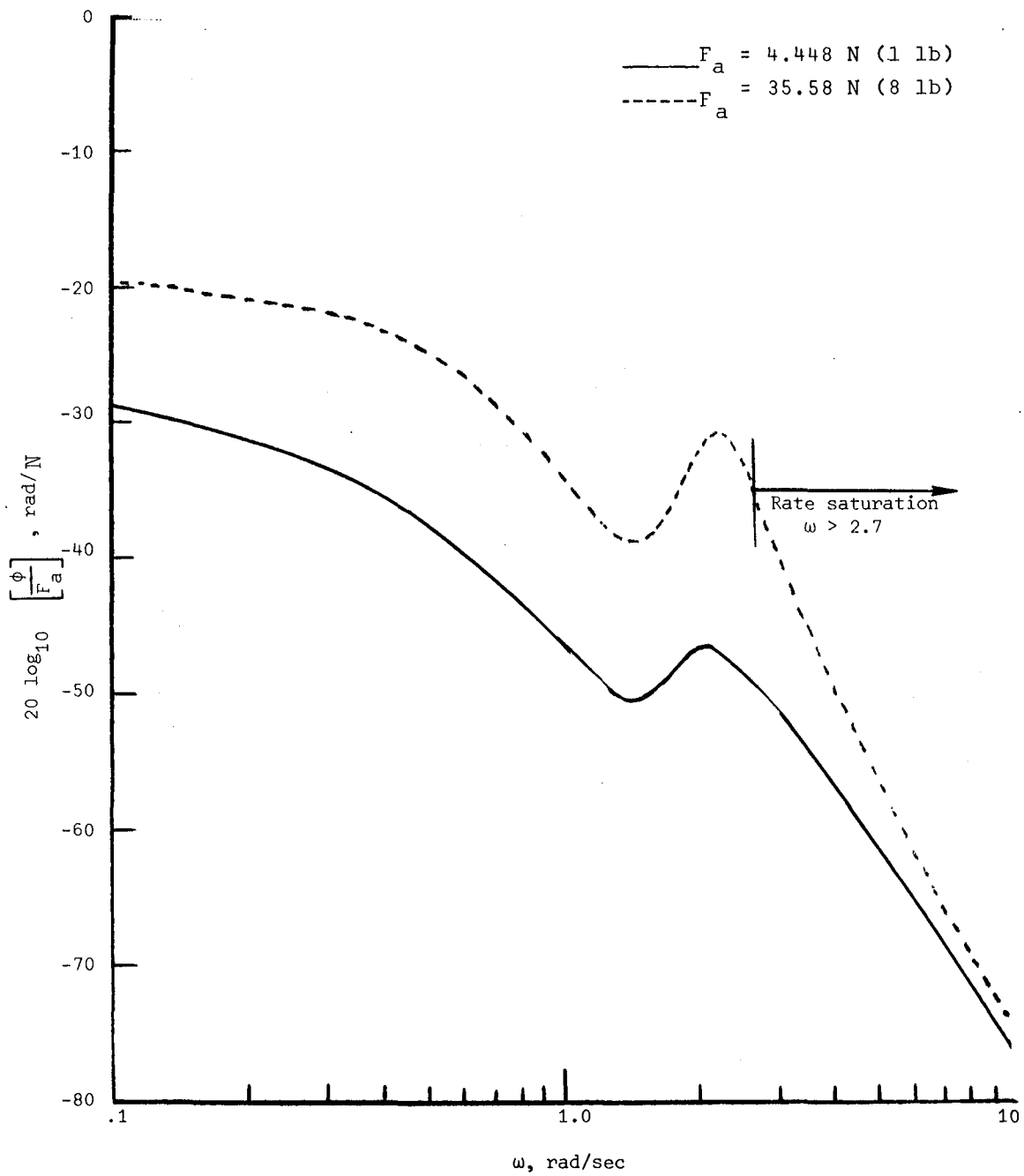
(a) Amplitude.

Figure 11. Frequency response of initial control system, in ground, effects, with pilot loop open.
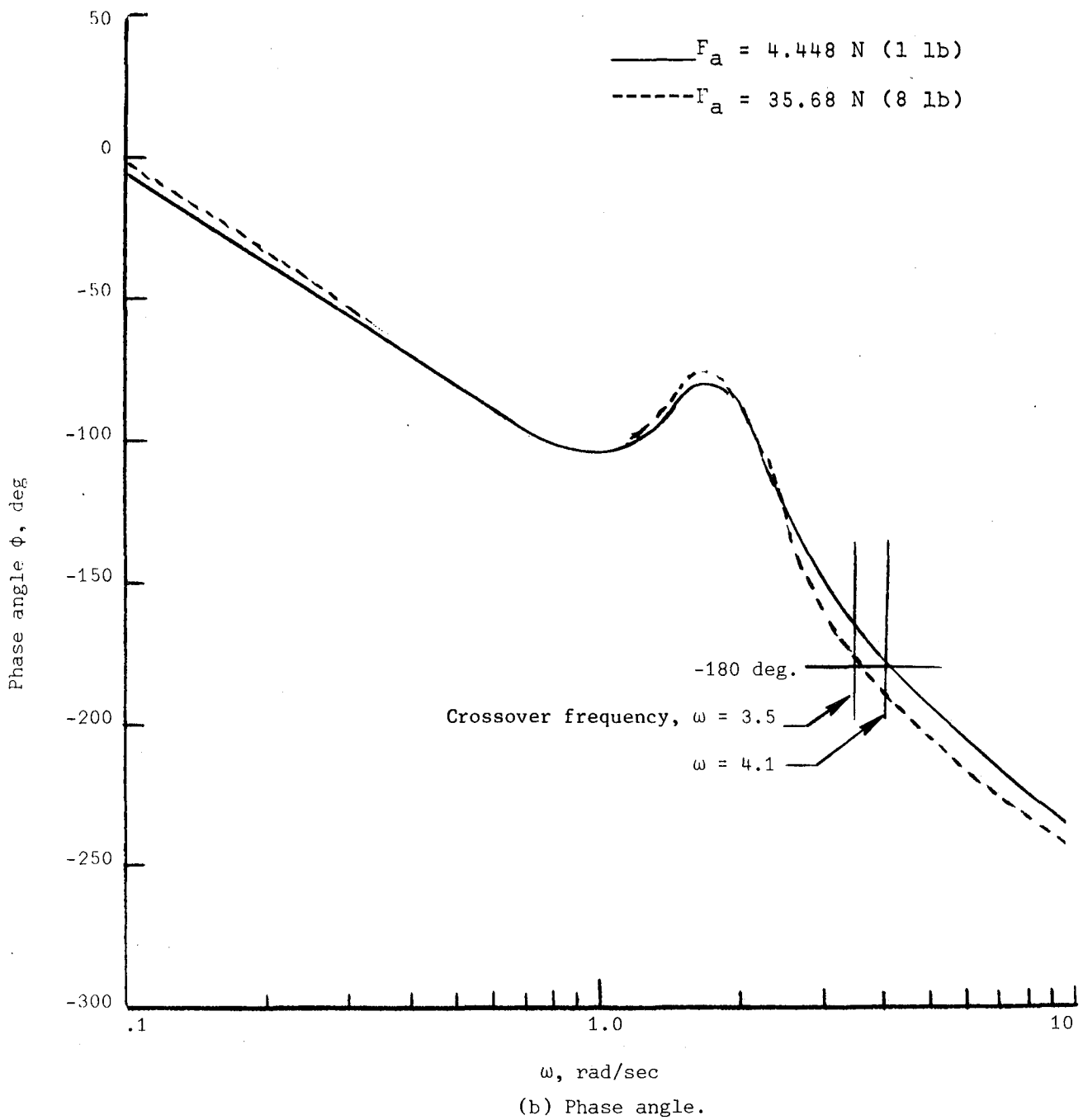
Figure 11. Concluded.
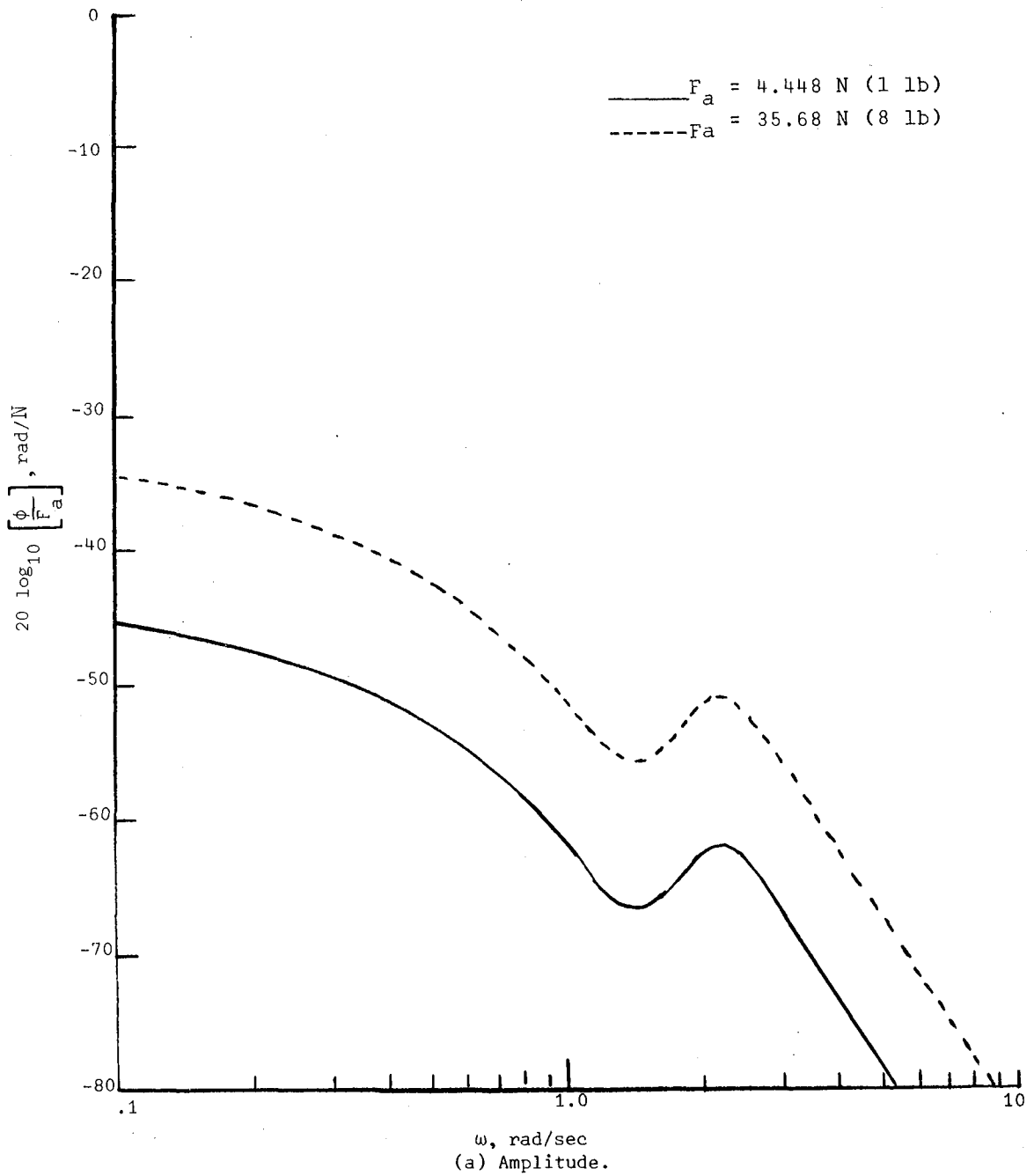
Figure 12. Frequency response of modified flight control
system configuration (MFCS) aircraft, in ground effects,
with pilot loop open.
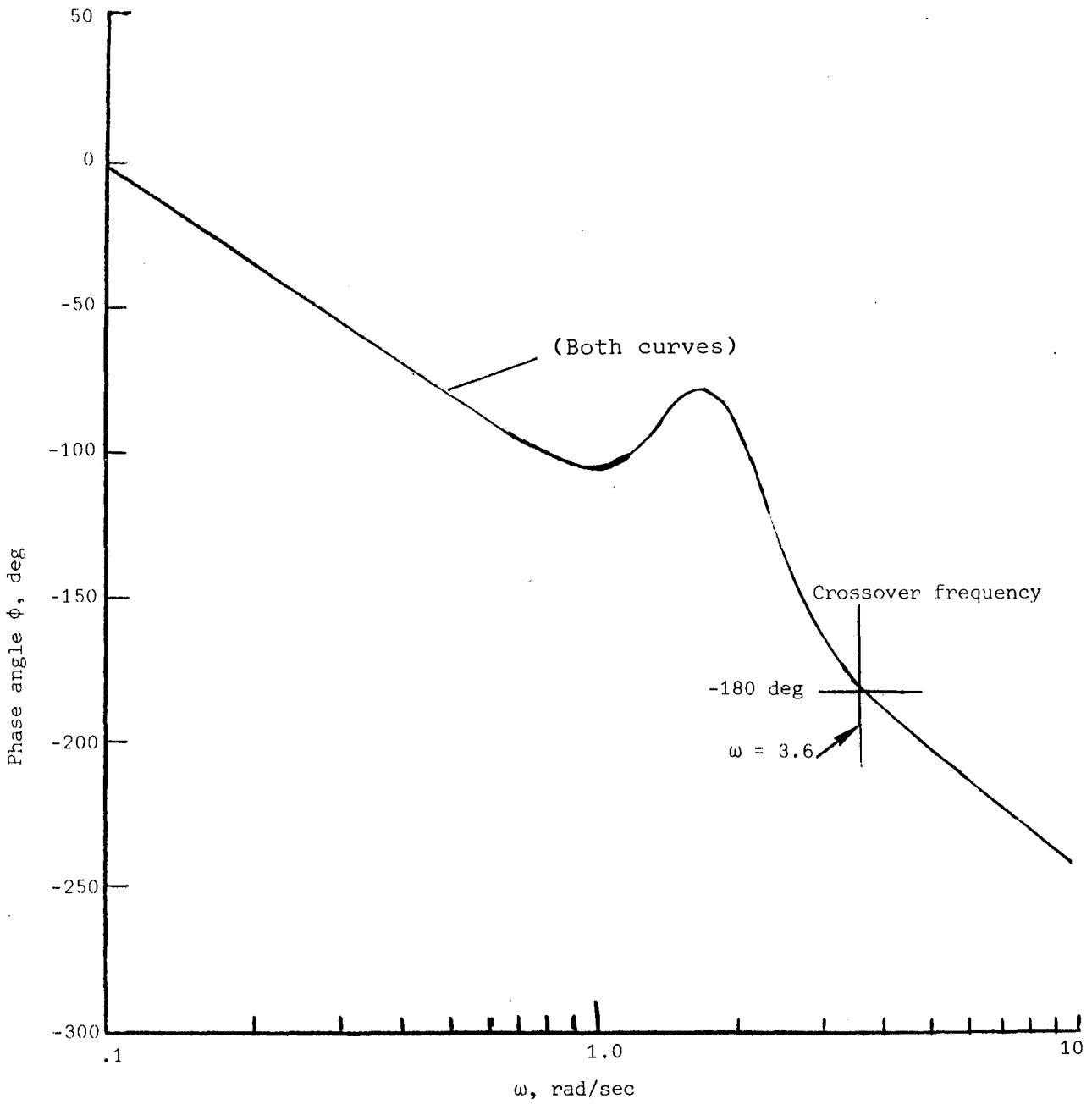
(b) Phase angle.

Figure 12. Concluded.
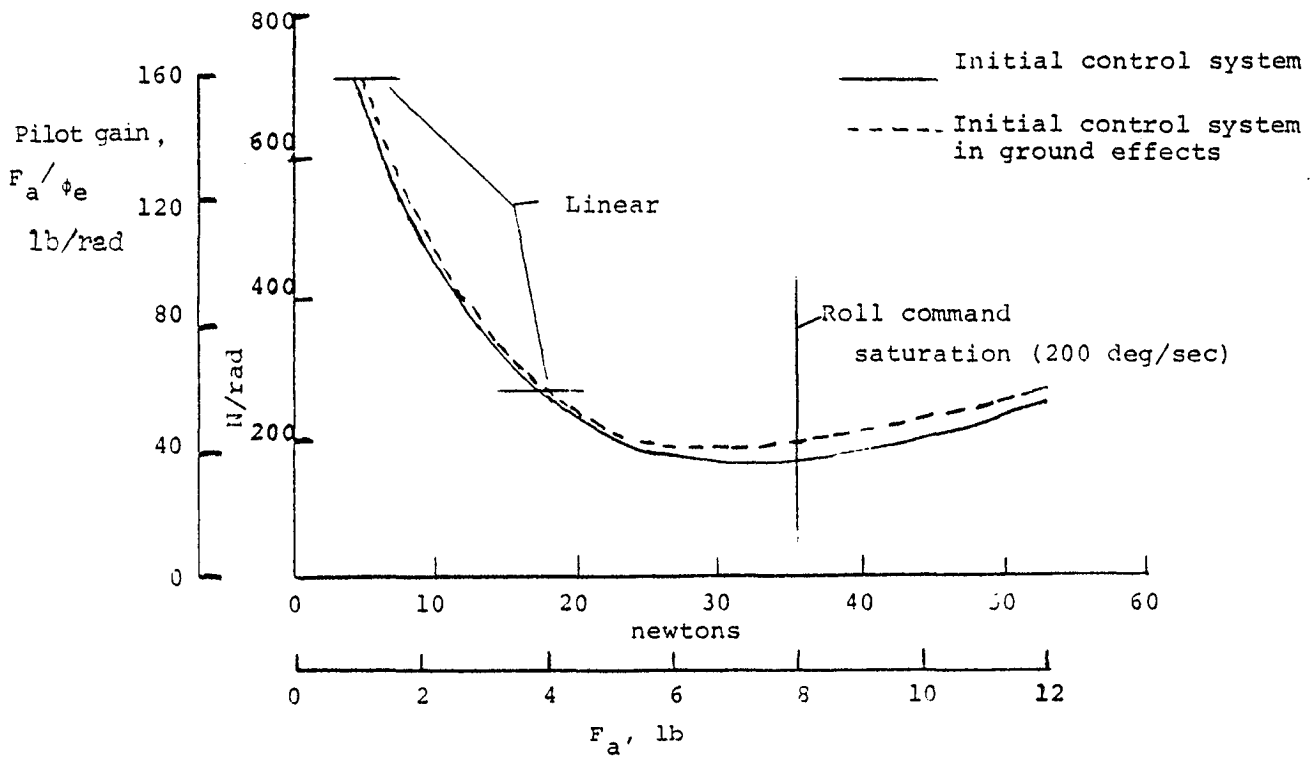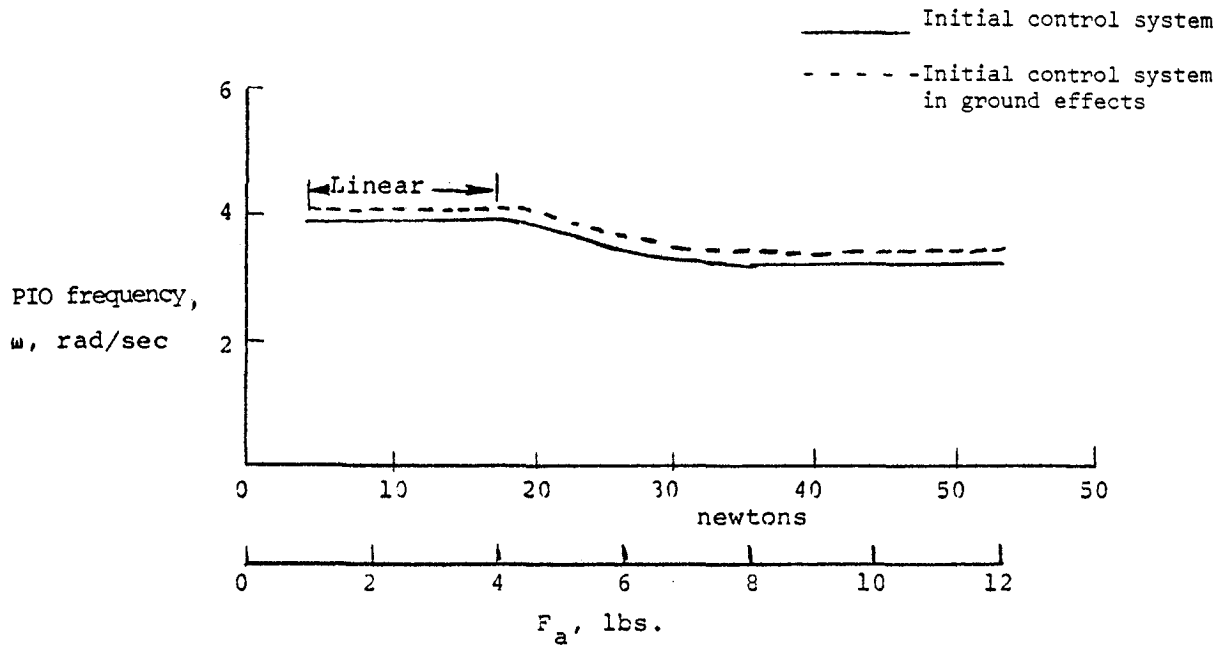
Figure 13. PIO frequency and minimum pilot gain required for PIO
versus input force for the initial control configuration in and
out of ground effect.
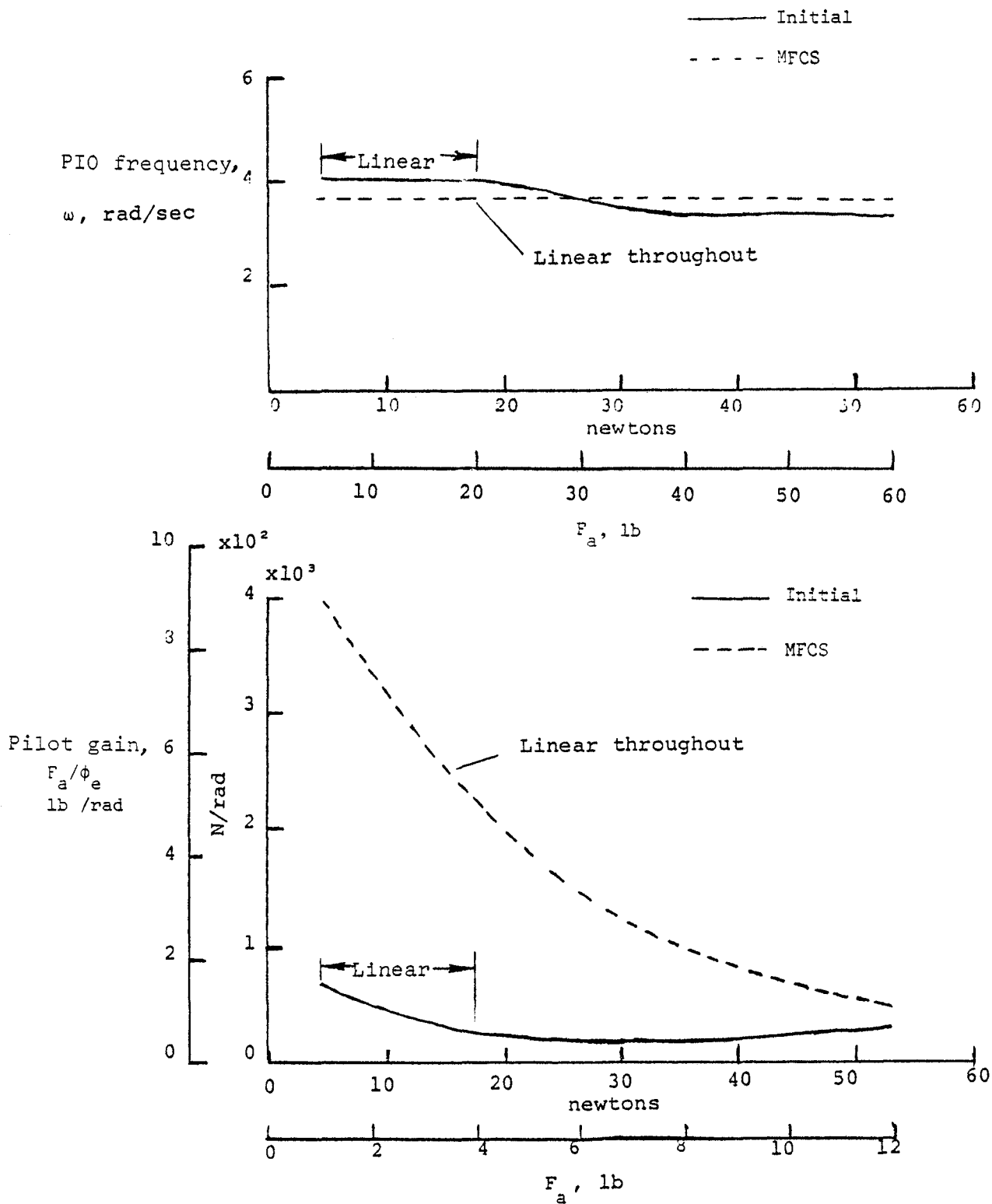
Figure 14. Comparison of the PIO frequency and minimum pilot gain in ground effect of the initial control configuration to the MFCS.
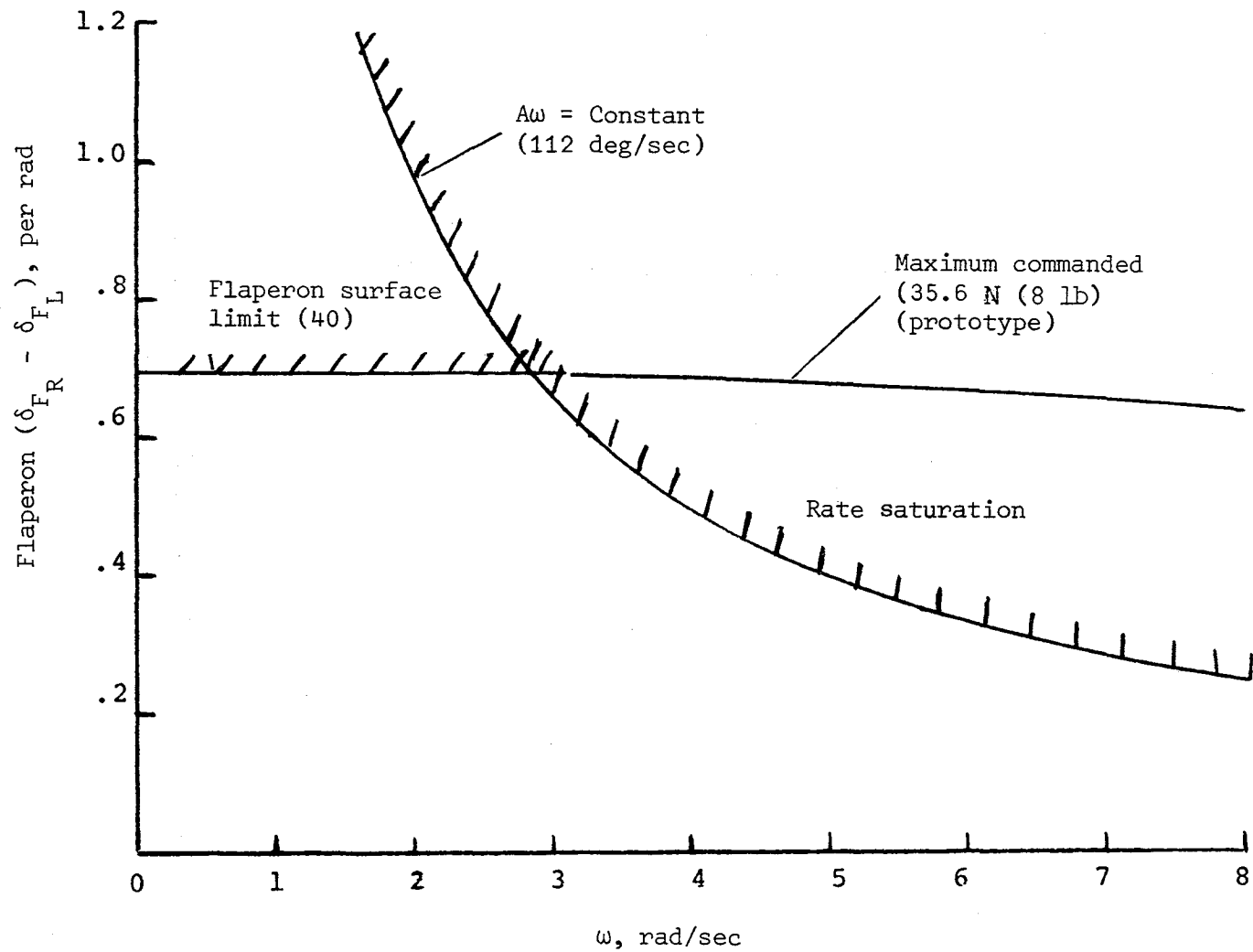
Figure 15. Comparison of mechanical limits of the intitial control system to commanded response of the aircraft in ground effects.

1.2

$A\omega$ = Constant
(112 deg/sec)

—————— F_a = 35.6 N (8 lb)

– – – – – F_a = 53.4 N (12 lb)

— · — F_a = 71.2 N (16 lb)

1.0

Flaperon surface
limits (40 deg.)

.8

Flaperon

$(\delta_{F_R} - \delta_{F_L})$,

rads

.6

Rate saturation

.4

.2

.0

0   1   2   3   4   5   6   7   8

ω, rad/sec
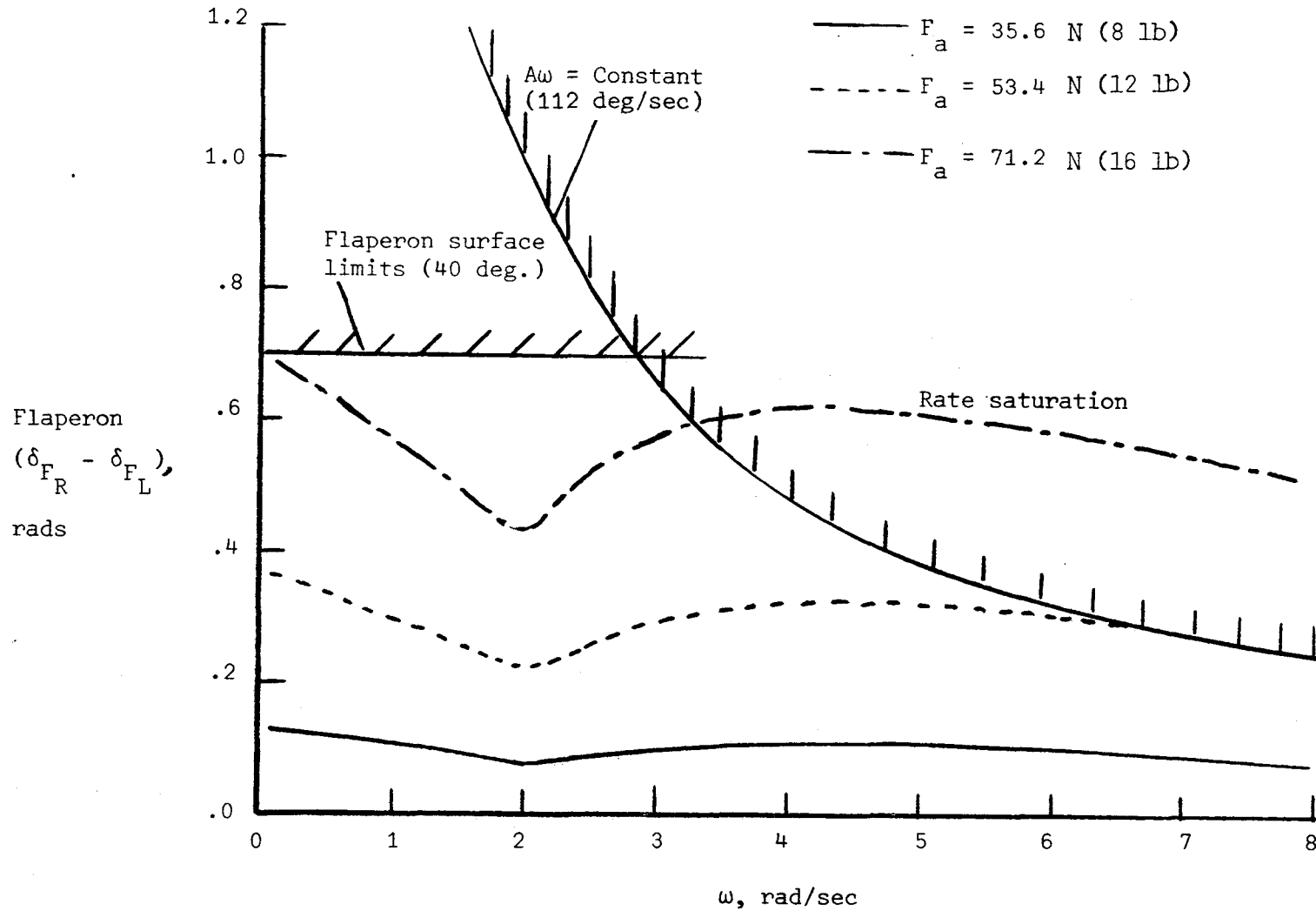
Figure 16. Comparison of mechanical limits of the modified flight control system (MFCS) to various commanded responses of the aircraft in ground effects.
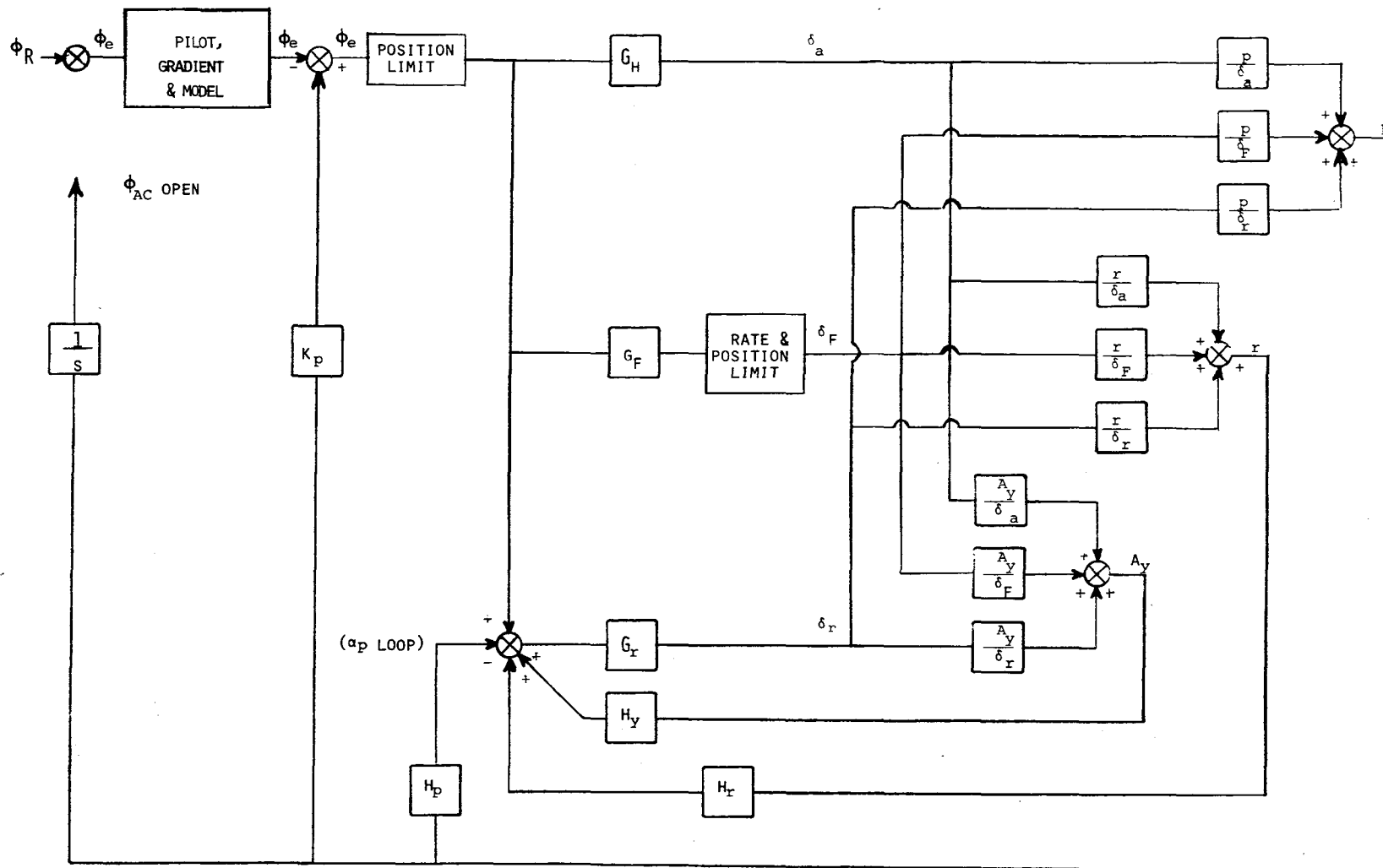
Figure 17. YF-16 functional block diagram of the lateral control system.
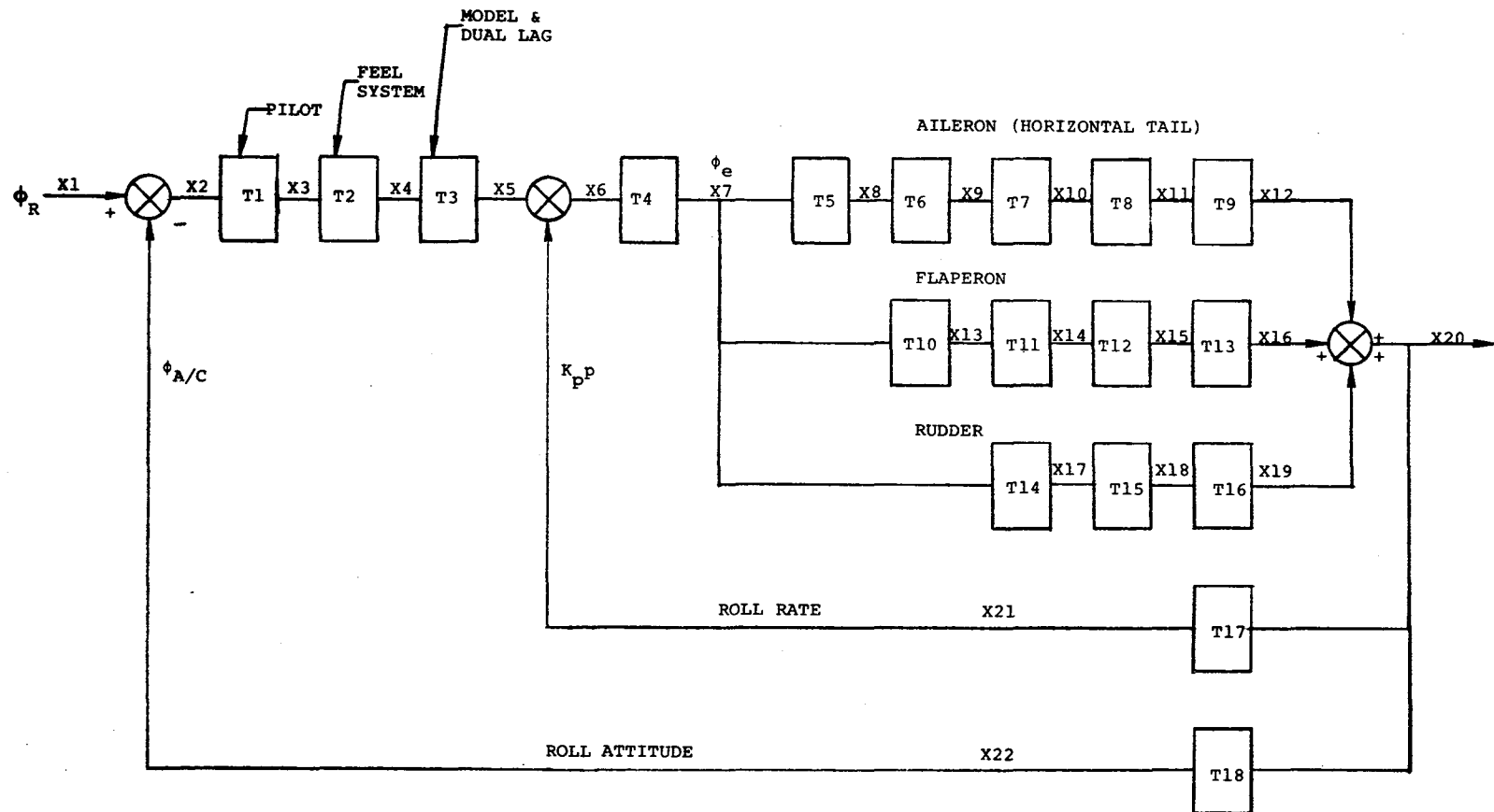
Figure 18.   YF-16 mathematical model.

1. Report No. NASA TM-72867	2. Government Accession No.	3. Recipient's Catalog No.
4. Title and Subtitle ANALYSIS OF A LATERAL PILOT-INDUCED OSCILLATION EXPERIENCED ON THE FIRST FLIGHT OF THE YF-16 AIRCRAFT		5. Report Date September 1979
		6. Performing Organization Code H-990
7. Author(s) John W. Smith		8. Performing Organization Report No.
		10. Work Unit No. 505-06-64
9. Performing Organization Name and Address NASA Dryden Flight Research Center P.O. Box 273 Edwards, California 93523		
		11. Contract or Grant No.
12. Sponsoring Agency Name and Address National Aeronautics and Space Administration Washington, D.C. 20546		13. Type of Report and Period Covered Technical Memorandum
		14. Sponsoring Agency Code

15. Supplementary Notes

16. Abstract

During the first takeoff of the YF-16 aircraft, a lateral-directional pilot-induced oscillation (PIO) occurred immediately at lift-off. The flight test data showed that the PIO lasted for 12 complete cycles at a frequency of approximately 0.7 cycle per second. Throughout the PIO, the control system was both position and rate saturated. The saturation, plus the normal aerodynamic and system lags, in conjunction with high pilot gain, was sufficient to sustain the PIO for 17 seconds.

Analytical studies, including ground effects, were conducted to investigate this particular control problem. In order to compare and assess potential improvements, two control systems were modeled; the original first flight or prototype aircraft system, and a modification of the prototype system, which essentially reduced the overall gain for the takeoff and landing phase.

In general, the overall system gain reduction of the modified flight control system was sufficient to avoid lateral PIO tendencies. Lowering the system gain reduced the tendency to rate saturate, which resulted in correspondingly higher critical pilot gains for the same control input.

17. Key Words (Suggested by Author(s)) Handling qualities Pilot-induced oscillations	18. Distribution Statement Unclassified – Unlimited STAR category: 08		
19. Security Classif. (of this report) Unclassified	20. Security Classif. (of this page) Unclassified	21. No. of Pages 54	22. Price*